Available online at www.CivileJournal.org

Civil Engineering Journal

(E-ISSN: 2476-3055; ISSN: 2676-6957)

Vol. 12, No. 02, February, 2026

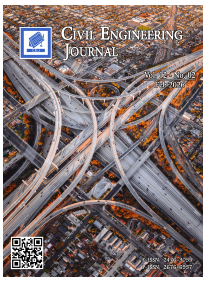

Structural Performance of Reinforced Concrete Voided One-Way Slab Under Static Loads

Fatima Hussien Awad [1*], Hussain A. Jabir [1]

[3] *Department of Civil Engineering, College of Engineering, University of Wasit, Al Kut 52001, Iraq.*

Received 10 October 2025; Revised 26 December 2025; Accepted 03 January 2026; Published 01 February 2026

Abstract

This study investigates the response of Reinforced Concrete (RC) voided one-way slabs under four-point bending, focusing on a novel and simple strengthening technique using embedded steel plates. Seven slab specimens were constructed with identical dimensions: 2000 × 600 × 130 mm. One specimen was a solid slab, serving as the control, while the remaining six were voided slabs. Among the voided slabs, one lacked a steel plate, and the other five were strengthened with steel plates of 1-, 2-, and 3-mm thickness. The primary objective of this study was to investigate whether the steel plate could compensate for the loss of strength and mitigate the impact of reducing the slab cross-section. The unstrengthened voided slab demonstrated substantial performance degradation compared to the reference solid slab, with 57% greater deflection at service load and significant reductions in ultimate load, stiffness, ductility, and toughness of about 23.5%, 25.4%, 10%, and 35%, respectively. Conversely, slabs strengthened with steel plates demonstrated a notable performance improvement. This was achieved by increasing flexural stiffness and reducing deflection at service load, with reductions ranging from 16% to 32% across the strengthened specimens. The percentage increase in ultimate strength ranged from 24% to 46% compared to the unstrengthened sample. Finally, a Finite Element Analysis (FEA) was performed using ABAQUS to validate the experimental results.

Keywords: Ductility; Steel Plate; Toughness; Voided Slabs.

1. Introduction

Structural support elements, such as slabs, are essential parts of a building. They create spaces within the structure and require large amounts of concrete. To guarantee stability and structural integrity, these slabs must be designed and built with maximum efficiency. The shift towards sustainable construction calls for optimizing slab design to reduce concrete use, as excessive consumption directly raises material costs and increases dead loads [1]. As a result, various efforts have been made to lower the self-weight of concrete slabs without sacrificing their flexural strength. Since aggregate interlock is key to maintaining shear resistance, not all interior concrete can be replaced. It must remain in the top part of the slab to form a compression block that resists flexural tension. Additionally, concrete in the lower section (tension zone) is vital for establishing a strong bond with the reinforcement and providing resistance. Furthermore, the top and bottom faces of the slab need to connect seamlessly to transfer stresses [2]. In 1990, Danish engineer Jørgen Breuning developed an innovative floor slab aimed at reducing self-weight by removing non-active concrete from its center [3]. Previous research demonstrates that embedding voids into slabs can lower the weight by 35–50%. When the dead load decreases, less steel reinforcement is required. Altering foundation design for lower dead loads also shortens construction time and reduces costs [4]. Moreover, voided slabs are regarded as more environmentally friendly because

* Corresponding author: Std2023203.F.H@uowasit.edu.iq

https://doi.org/10.28991/CEJ-2026-012-02-024

they use less cement. This reduction is significant, considering that producing one ton of cement emits roughly 500 kg of CO_2, thereby decreasing the structure's overall carbon footprint [1, 5]. Studies indicate that slabs with voids retain about 87% of the flexural stiffness of equivalent solid slabs. This implies that a slab with voids may deform or bend more under service loads than a solid slab. However, deflection depends on the material's stiffness-to-bending resistance ratio.

In one-way slabs, load is transmitted differently from two-way slabs, as these forces are transmitted to supports in a single direction. The presence of voids in this direction could disrupt the load-transmission path, potentially leading to sudden collapse. Therefore, greater attention should be given to the design of voided slabs for one-way support resting. Recently, numerous experimental studies have been conducted to investigate the impact of voids on slabs, especially their size and former shapes [6-14]. Although Reinforced Concrete (RC) voided one-way slabs offer significant benefits such as reduced self-weight, environmental impact, and material consumption compared to solid slabs, their structural performance, including load-bearing capacity, stiffness, toughness, and ductility, decreases under static loading, resulting in more deflection and quicker crack formation caused by the concentration of stresses due to the presence of voids. Multiple solutions have been proposed to address these issues, including the use of Glass Fiber Reinforced Polymer (GFRP) for strengthening [15, 16]. This approach has been demonstrated to enhance the toughness and durability of bridge deck slabs.

Jamal & Vijayan [17] examined bubble deck slabs reinforced with GFRP sheets containing existing elliptical voids subjected to uniform load. Numerical analysis using ANSYS software was performed to evaluate slabs and reduce deformation. The study analyzed equivalent stress, directional deformation, and overall deformation of bubble deck slabs with and without GFRP sheets, employing a 180 × 240 mm elliptical void filled with High-Density Polyethylene (HDPE) elliptical balls, and slabs with dimensions of 1730 × 1350 × 230 mm. Results indicated that bubble deck slabs with elliptical voids and GFRP sheets increased load-carrying capacity and decreased deflections compared with slabs with elliptical voids alone. Additional testing by the authors in Aman et al. [18] revealed that multiple CFRP layers on slabs improved resistance to external forces. The relationship between deflection and coating count is inverse. Additional research was conducted on seven 700 × 450 × 80 mm air-bubbled RC slabs [19]. CFRP strips were used to repair the slabs after they were burned and loaded until they failed, with one slab remaining as a reference. The recovered Bubbled Slab (BS) supported 79%–105% of the ultimate load of the reference slab and had flexural strength comparable to that of the reference sample. The shear strength of the concrete slab is determined by its effective mass because of the plastic bubbles. Therefore, bubbled deck slabs have less shear strength than solid slabs. The voided slab has 60–80% of the shear strength of a Steel Slab (SS) of the same depth, according to theoretical calculations. Thus, the shear capacity of all bubbling deck slabs needs to be decreased by 0.6.

Abdulkhaliq & Ahmed [20] conducted a study on six one-way slabs, each measuring 2,600 mm in length, 600 mm in width, and 150 mm in depth. These slabs are reinforced with GFRP bars, strengthened by embedded steel I-sections. Five slabs were BS, one of which was unstrengthened, and they were compared with the control Solid Slab. The study investigates the influence of inclusion voids and GFRP reinforcement on ultimate load, stiffness, and deformation, comparing them to the control SS. They also examined how steel I-section strengthening enhances BS behavior. The result indicates BS had a 15% reduction in ultimate load capacity and a roughly 28%–88% increase in the range of deformations (including deflection, strains, and cracks) compared to solid slabs. In contrast, the specimen performance was considerably enhanced by the use of steel I-sections as internal reinforcement compared with unreinforced SS and BS. The ultimate load capacity increased by roughly 121% and 179%, flexural stiffness increased by about 197% and 272%, and deflection decreased by about 52% and 87% at the same load level.

Finally, the study reported that the unreinforced slabs exhibited a brittle failure mode, failing in the tension zone under flexural stresses. Strengthening with steel I-sections altered the failure mode from brittle tension to brittle compression due to its contribution to strengthening and withstanding stresses in the tension zone. Another study reported that shear reinforcement increased the ultimate load of the voided slab, as demonstrated in Yaagoob & Harba [21]. Some studies have strengthened the voided slab using reactive powder concrete and reported flexural strengths higher than those of ordinary concrete slabs [22, 23].

A study by Ismael et al. [24] examined five voided one-way ferrocement specimens. The slab was subjected to a four-point load until failure. Plastic bottles were used to create voids within the ferrocement slabs. A specific focus was on fiber percentage and the void ratio of waste plastic bottles. The research results indicated that the presence of voids in the slabs decreased their dead load as well as their stiffness and ductility compared to the solid slab. Moreover, it was revealed that the ultimate load capacity decreased by roughly 18.5% when two lines of hollow plastic tube were used compared to the solid slab. To mitigate these impacts, 1% of Polypropylene (PP) fibers were employed. The findings indicated that adding PP fibers was an effective method to improve the overall flexural stiffness of hollow slabs, making them more similar to the original slab.

Generally, few studies have considered the strengthening of RC voided one-way slabs. Furthermore, most of the strengthened methods increased stiffness only and exhibited bilinear elastic behavior until failure, with brittle failure

often observed. Therefore, a new solution should be developed to enhance the overall behavior of a voided one-way slab, such as ductility and toughness. The current study presented a new, simple solution to improve the behavior of voided one-way slabs using steel plates to address these knowledge gaps. Steel plates were embedded in each voided slab. The steel plate's thickness was variable (1, 2, and 3 mm). The suggested method's activeness was confirmed through an experimental comparison with a voided slab without steel plates and a solid slab. Subsequently, a Finite Element Analysis (FEA) was implemented to verify the improvement mechanism of steel plates. Two parameters were evaluated: plate thickness and arrangement. Additionally, this research includes a detailed evaluation of the voided slabs' results using six criteria: toughness, stiffness, ductility index, strain at ultimate load for tension bar and steel plates, ultimate load, and deflection at ultimate load.

2. Experimental Program

2.1. Specimen Preparation

Constructing and testing seven slab specimens with measurements of 2000 × 600 × 130 mm (length, width, and thickness) was a part of the experimental program. Figure 1 illustrates the details and dimensions of voided slabs. One slab served as a solid control specimen (reference specimen). The other six slabs were voided by 27 cuboid styropor inserts measuring 150 mm × 150 mm × 70 mm (length, width, and thickness) placed within the slab between the reinforcing layers. The concrete ribs were 50 mm thick in both the transverse and longitudinal directions, and 30 mm-thick concrete flanges were below and above the inserts, as displayed in Figure 1-b. Five specimens were reinforced with steel plates of varying thicknesses (1, 2, and 3 mm) to improve their behavior (see Figures 2-a and 2-b). Three slabs had two steel plate strips of varying thicknesses and were named V1, V2, and V3, and two slabs had four and six steel plates and were named V12 and V111, respectively. The first symbol represents the slab type, and the second represents the thickness of the steel plate. One voided specimen without a steel plate was designated V0. To acquire a comprehensive summary of the tested slabs, including their details and descriptions, refer to Table 1.

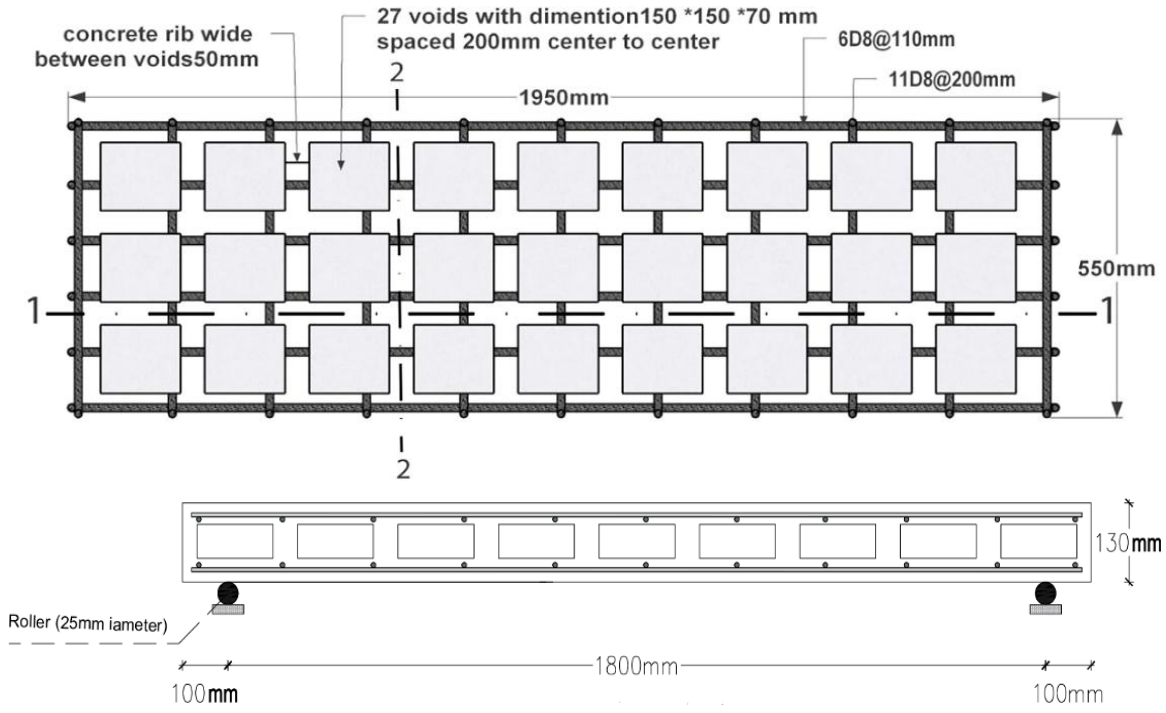

(a)

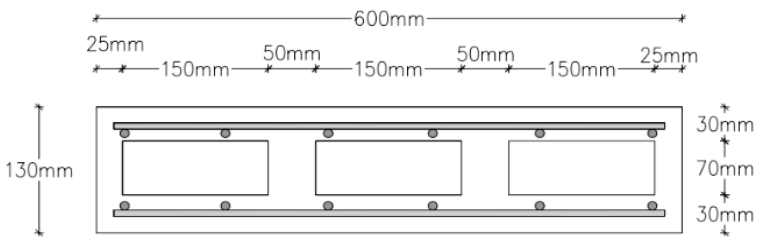

(b)

Figure 1. Details of the voided slab (a) section (1-1) longitudinal cross-section in voided slab, including voids and reinforcement (b) section (2-2) transverse cross-section of voided slab

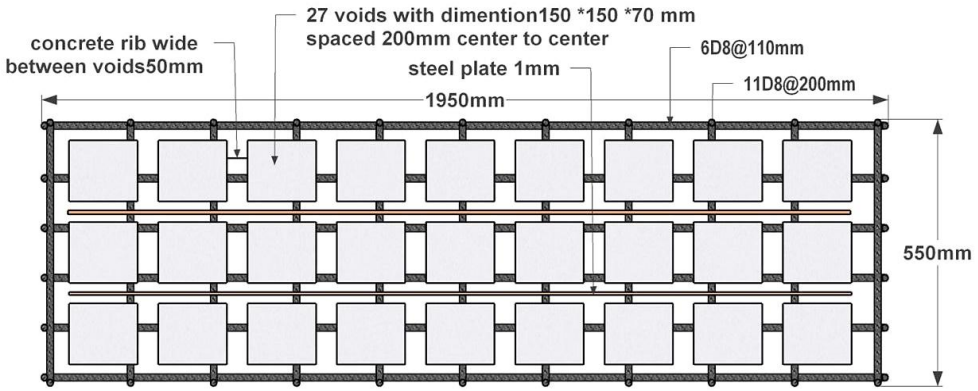
concrete rib wide
between voids50mm
27 voids with dimention150 *150 *70 mm
spaced 200mm center to center
steel plate 1mm
6D8@110mm
11D8@200mm
1950mm
550mm

(a)

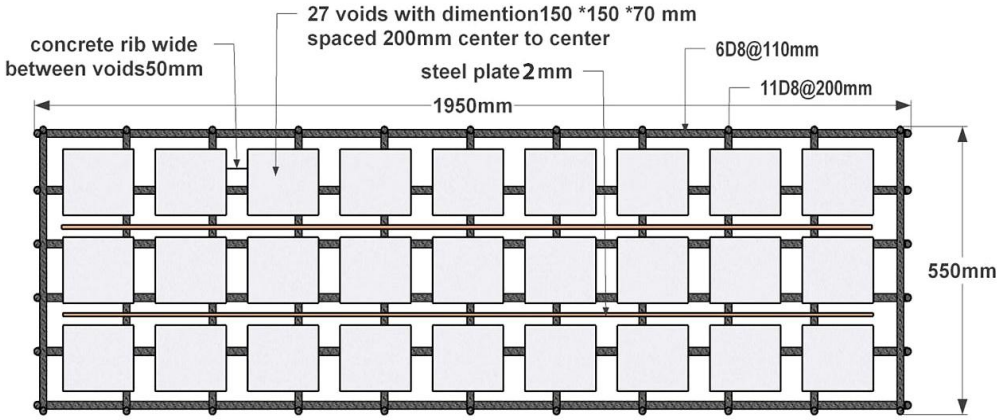
concrete rib wide
between voids50mm
27 voids with dimention150 *150 *70 mm
spaced 200mm center to center
steel plate 2mm
6D8@110mm
11D8@200mm
1950mm
550mm

(b)

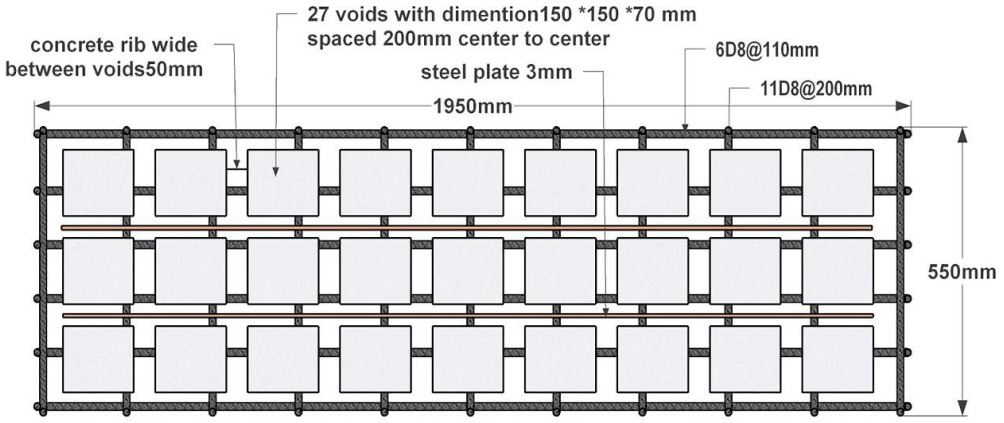
concrete rib wide
between voids50mm
27 voids with dimention150 *150 *70 mm
spaced 200mm center to center
steel plate 3mm
6D8@110mm
11D8@200mm
1950mm
550mm

(c)

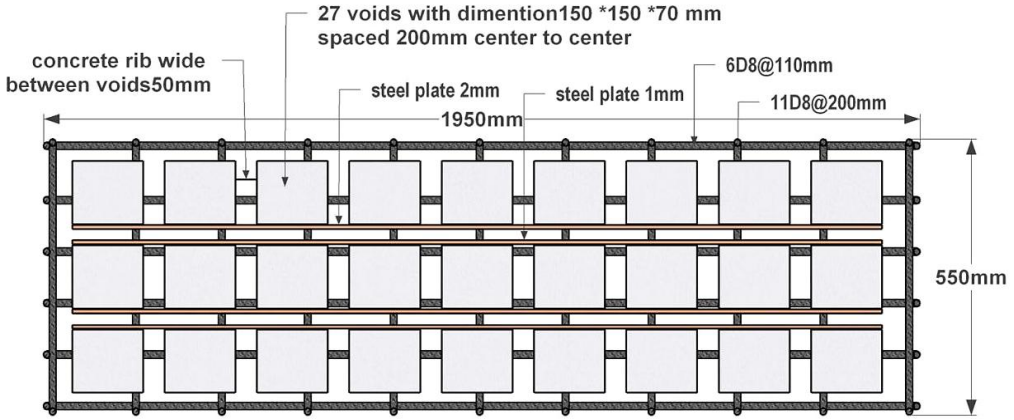
concrete rib wide
between voids50mm
27 voids with dimention150 *150 *70 mm
spaced 200mm center to center
steel plate 2mm
steel plate 1mm
6D8@110mm
11D8@200mm
1950mm
550mm

(d)

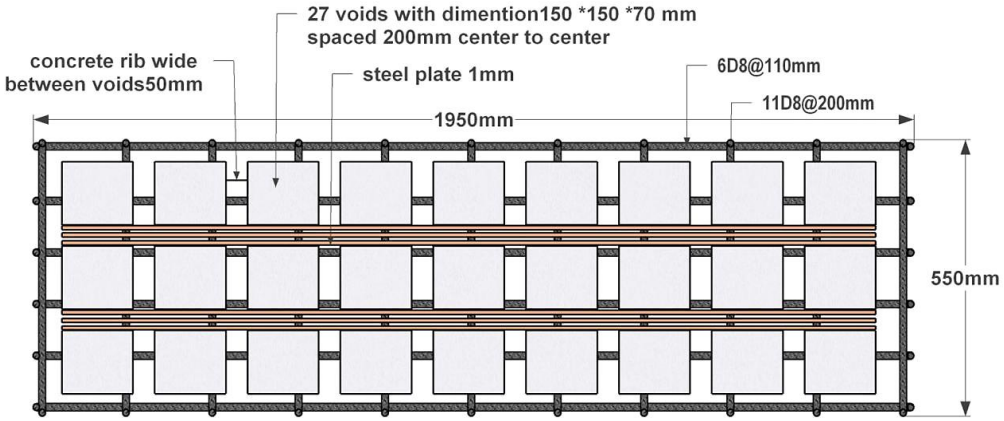

(e)

Figure 2. Geometric and reinforcement details of voided slabs with steel plates (a) arrangement of voids and steel plates inside the V1 specimen (b) arrangement of voids and steel plates inside the V2 specimen (c) arrangement of voids and steel plates inside the V3 specimen (d) arrangement of voids and steel plates inside the V12 specimen (e) arrangement of voids and steel plates inside the V111 specimen.

Table 1. Characteristics of the tested slabs

Number	Designation	Cross-section type	Thickness of steel plates (mm)	Number of steel plates in the samples
1	S	Solid	-	-
2	Vo	Voided	-	-
3	V1	Voided	1 mm	2
4	V2	Voided	2 mm	2
5	V3	Voided	3 mm	2
6	V111	Voided	1 mm	6
7	V12	Voided	1 & 2 mm	4

To satisfy the required development length, a total of 1950 mm of steel plate was inserted along the specimen's length. The steel plates placed directly between the top and bottom layers of steel reinforcement were 68 mm high. The yield strength of the steel plates with thicknesses of 1, 2, and 3 mm was 305 MPa on average. The steel plates had two rows of 15 mm-diameter holes to anchor them within the slabs and allow aggregate to flow along their length. The holes were evenly spaced and staggered, with a 200 mm Center-to-Center (C-to-C) spacing and a 25 mm C-to-C gap between the two rows. It is worth noting that Lameiras et al. [25] proposed using holes to secure the plates. They performed pull-out experiments after embedding steel plates reinforced with glass fibers into the concrete slab. According to them, the holes' diameter should not be smaller than the aggregate's maximum size. Additionally, they identified that the bond's strength increased with the number of holes.

Conversely, no suggestions were made regarding the distance between holes. The diameter of the holes chosen for this study, which was nearly 50% greater than the aggregate's maximum size of 10 mm, is suitable for forming the smallest cut area from plates. This diameter is approximately 22% of the steel plate's height. As illustrated in Figure 3, the spacing between holes in a single line was roughly 2d, so bonding the plates into the slab was to be done at intervals of d, or the distance between two consecutive holes. Figure 4 illustrates detailed information for the steel plates used. The slabs were reinforced with two mesh reinforcement layers at the bottom and top. In the short direction, the primary reinforcement was 6Ø8 at a 110 mm C-to-C spacing, while the secondary reinforcement was 11Ø8 at a 200 mm C-to-C spacing, distributed perpendicularly. The upper layer was configured in the same way. Figure 3 depicts the information about the reinforcement. The ultimate strength was 577 MPa, whereas the yield strength of rebar Ø8 was 516 MPa. The effective depth (d) is 112 mm, and the net concrete cover is 10 mm. To ensure the same concrete grade is used in each slab, the same batch of self-compacting concrete, which flows smoothly into small gaps between voids, is used to cast the specimens. As a result, an external vibrator is not necessary. Figure 5 presents the specimen before and after casting. Several trial mixes were produced, with an intended compressive strength of 40 MPa. The mix design was chosen to meet ASTM specifications. Thus, four tests, slump flow, penetration, J-Ring, and T50, were conducted to assess each trial mix's fresh properties. The gravel aggregate was scrubbed angular, with an ultimate size of 10 mm. Figure 6 presents the grading analyses of fine and coarse aggregates, with Ordinary Portland cement used in the mix. Tables 2 and 3 depict the chosen mixing ratio and the fresh properties of the mixture, respectively.

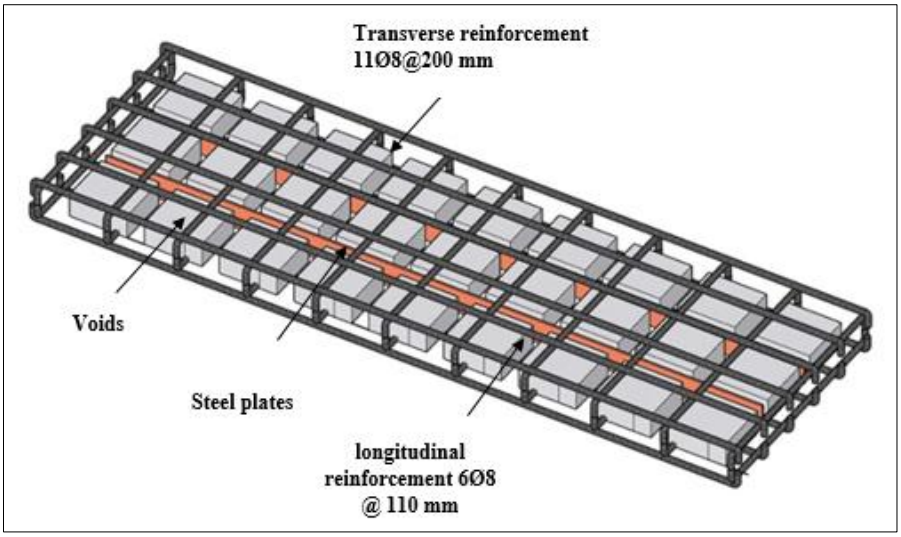

(a)

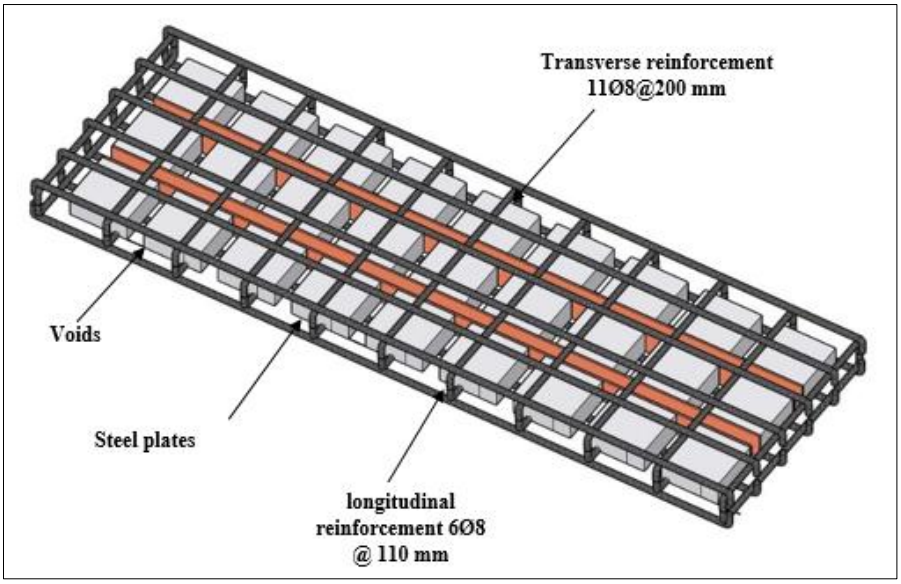

(b)

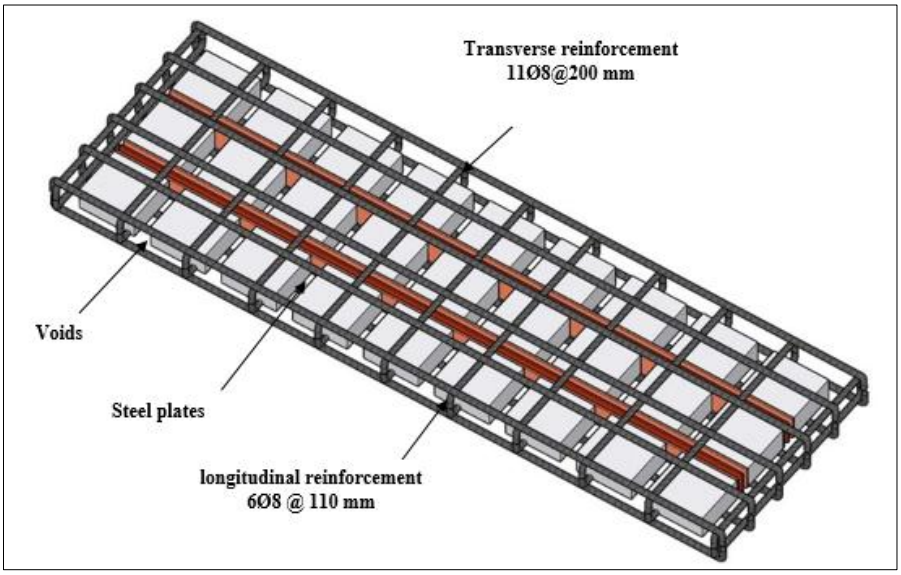

(c)

Figure 3. Details of reinforcement in 3D for voided specimens with steel plates (a) details of reinforcement in 3D view for V1, V2, and V3 specimens (b) details of reinforcement in 3D view for V12 specimen (c) details of reinforcement in 3D view for V111 specimen.

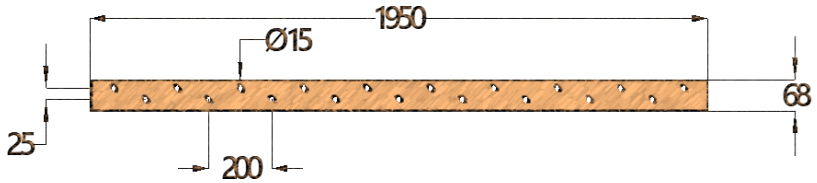

Figure 4. Details of steel plates (all dimensions in mm)

Figure 5. Preparation and casting stage of the slab specimens

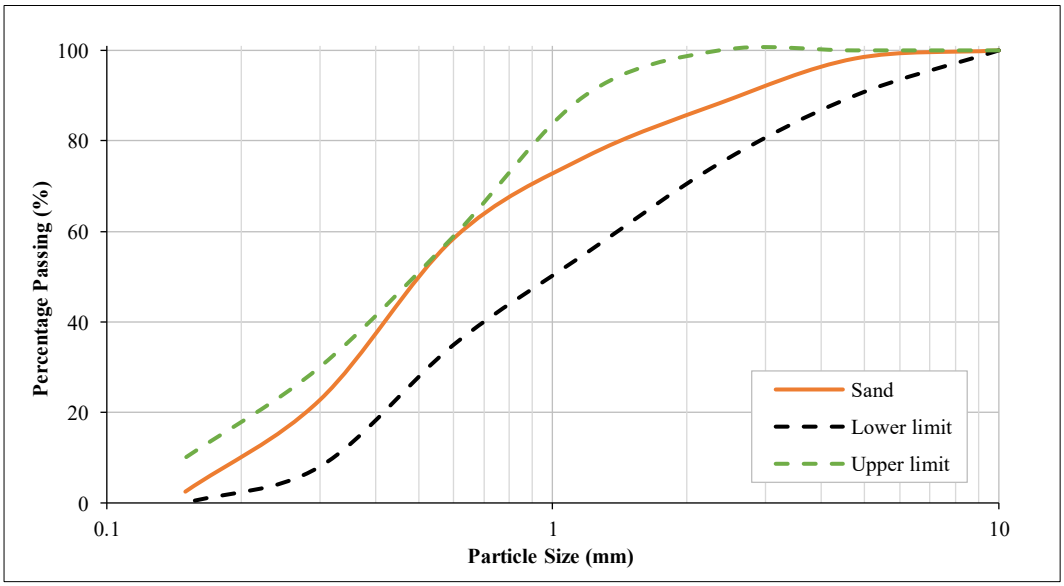

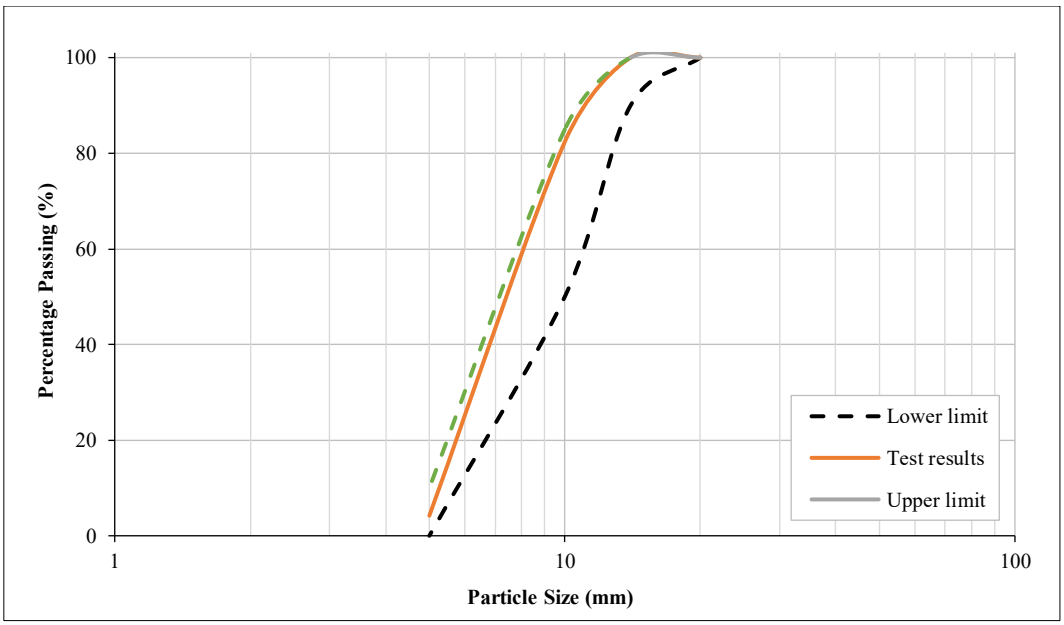

Figure 6. Sieve analysis of fine and coarse aggregates

Table 2. The self-compacting concrete's mixing ratio

Material	Quantity of materials
Fine aggregate (kg/m^3)	1060
Cement (kg/m^3)	400
Water (kg/m^3)	185
Water/cement ratio	0.463
Coarse aggregate (kg/m^3)	586
Superplasticizer (kg/m^3)	11.4
Limestone Powder (kg/m^3)	70

Table 3. The chosen mixing ratios' fresh properties

Test	Result	ASTM
Slump Flow (mm)	625	480-680
Penetration (mm)	5	0-10
J-Ring (mm)	45	0-25* 25-50**
T_{50} (sec)	5	2-5

* No visible blocking; ** Minimal to noticeable blocking,

2.2. Test Configuration and Instrumentation

Figure 7-c illustrates a four-point bending load that was used to test all slabs after twenty-eight days of casting. A manual hydraulic jack was used to apply the load to the steel beam, and two equal line loads, spaced 400 mm apart, were then used to distribute and transmit the load to the slab. A 5 kN step load was applied gradually until collapse. The specimens were positioned on the 1800 mm clear-span testing frame, which was supported by roller bars at two edges. As a result, during the test, the specimens' corners were free to be lifted. A load cell was placed between the plating load and the hydraulic jacks to absorb the applied load, as displayed in Figure 7-a. Additionally, the specimens' central deflection was recorded using a two-linear Variable Differential Transducer (LVDT), situated at the span's midpoint and 350 mm away from the face of the supports, below the tension face of the samples, and attached to the lower steel beams of the testing machines (see Figures 7-b and 7-c).

(a)

(b)

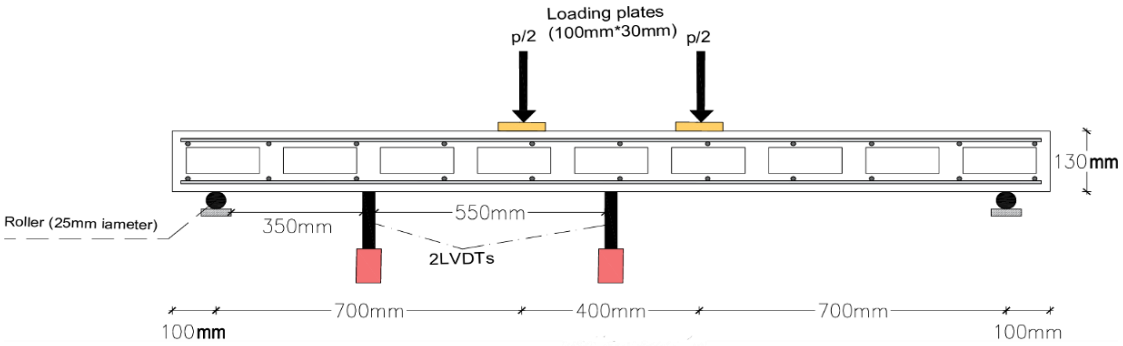

(c)

Figure 7. Test setup (a) the specimen within the testing frame (b) LVDTS arrangement (c) the test setup graphical representation

Moreover, electric strain gauges are installed on the central bottom longitudinal bars. Simultaneously, three strain gauges were attached to the steel plate at the mid-span, under the point load position, and 350 mm away from the support. The strain-gauge locations on the steel plate are illustrated in Figure 8. Finally, every piece of equipment used to observe the test outcomes was connected to the Data Taker G85. This data logger took readings every second during the test and subsequently sent them directly to a computer. Figure 9 presents a flowchart outlining the complete work for voided slabs with steel plates of different thicknesses.

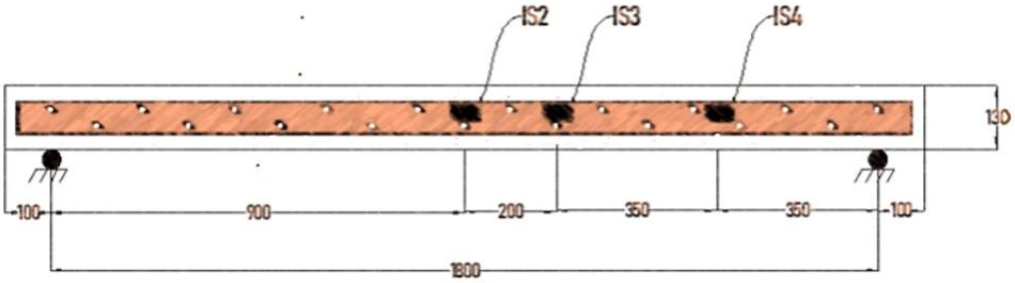

Figure 8. Locations of strain gauges (all dimensions in mm)

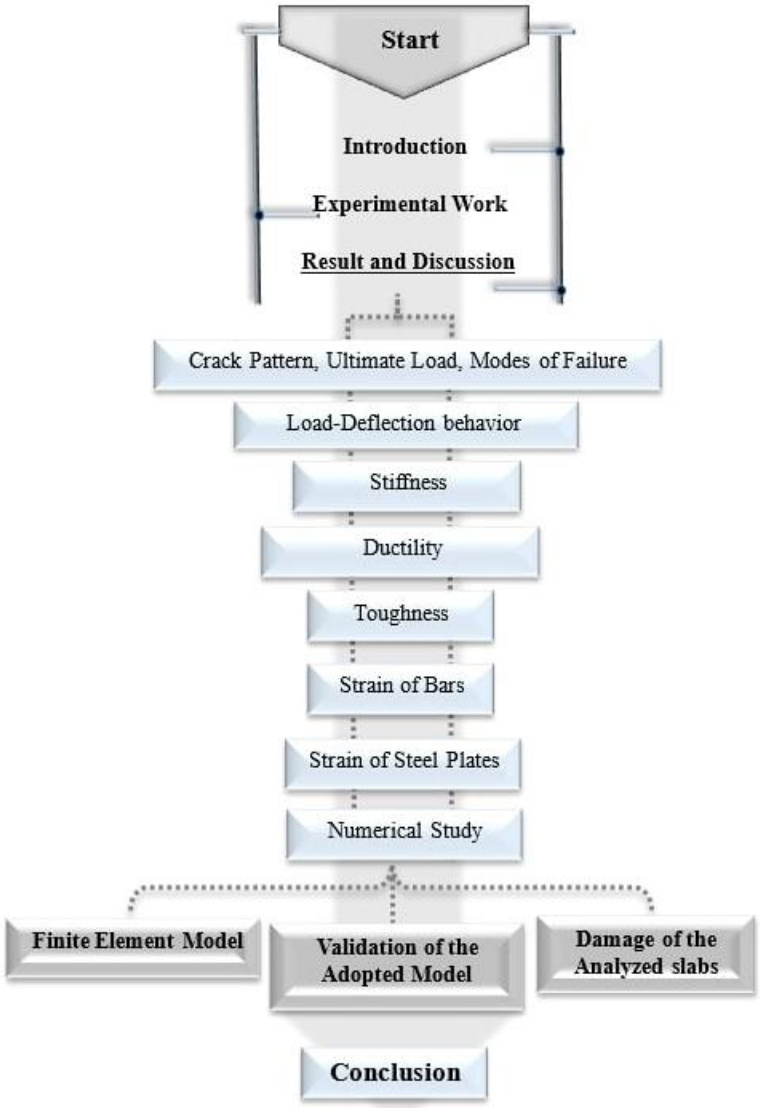

Figure 9. The flowchart describes the whole experimental design

3. Results of the Test and Discussion

3.1. Cracking Pattern, Ultimate Load, and Failure Mode

Figure 10 illustrates the arrangement and distribution of cracks at failure for each specimen. The thickness and arrangement of the steel plates influence the crack patterns in the voided specimens. The first flexural crack appeared on the specimen's tensile face when tensile stresses surpassed the concrete's modulus of rupture, in the middle section at the maximum moment. The initial bending cracks were observed at roughly 12.8 kN for the solid specimen and between 9.8 and 10.3 kN for the voided samples with and without a steel plate. As expected, the voided specimen without a steel plate cracked at lower loads than the control slab due to the direct reduction in its moment of inertia resulting from removing concrete to create voids. Conversely, the first crack was delayed when steel plates were used. Regarding crack development for all slabs, the cracks gradually spread across the width of the slab, moving parallel to

the supports. Increasing the static load caused flexural cracks to form parallel to the initial crack and extend progressively throughout the slab's thickness. Figures 10-a and 10-b clearly demonstrated that the solid specimen developed more cracks than the voided specimen without a steel plate, and also indicated larger crack widths in the V0 slab, allowing rapid propagation from the solid to the void zone. This may be explained by the solid specimen's ability to absorb more energy before failure, as well as the reduced load capacity of the V0 slab. The analysis also includes the remaining specimens with a steel plate. It was observed that the number of cracks increased and spread over a larger area compared to the V0 specimen. Cracks appeared intermittently during formation, initially vertical and concentrated in the center zone before propagating towards the support. As the load increased, additional cracks developed at an angle due to pressure that caused the material to slide, spreading towards the nearest concentrated load and penetrating the compression zones of the slab at the loading point, owing to the greater load capacity, as illustrated in Figures 10-c to 10-g. The V12 slab exhibited more cracks than the V111 slab, owing to its greater load-bearing capacity. Additionally, as presented in Figure 7, the cracks in the specimens without steel plates (S, V0) remained parallel and vertical until failure. In contrast, specimens with steel plates V1, V2, V3, V111, and V12 exhibited curved cracks that extended across the slab thickness. With increasing load, crushing occurred on the compression face for each specimen except the solid one, due to the thin flange of the voided specimen, leading to stress concentration at the top face of the slabs.

Side face

Tension face

(a)

Side face

Tension face

(b)

Side face

Tension face

(c)

Side face

Tension face

(d)

Side face

Tension face

(e)

Side face

Tension face

(f)

Side face

Tension face

(g)

Figure 10. The pattern of cracks at collapse (a) sold slab (S) (b) voided slab (V0) (c) Voided slab (V1) (d) voided slab (V2) (e) voided slab (V3) (f) voided slab (V111) (g) voided slab (V12)

Table 4 presents the ultimate loads for all samples. The load capacity of slabs with voids (V0) is reduced by 23.5% compared to the reference slab, consistent with prior research [8, 26]. The decrease can be attributed to the reduced cross-sectional area and increased stress concentration in the flange and rib regions around the voids, which accelerate crack development compared to solid materials. Specifically, it reduced the slab's moment of inertia, thereby reducing its ability to resist deformation and bending under load, as observed in specimens including steel plates. In the specimen with a thickness of 1 mm (V1), there is an observed reduction in ultimate load compared to the solid specimen. However, the decrease is not as substantial, about 5.5%. The remaining specimen recorded a slight increase compared to the reference slab, with values of approximately 7.3%, 12%, 4.5%, and 11.5% for V2, V3, V111, and V12, respectively. Therefore, the presence of a steel plate within the voided slabs substantially improves the ultimate load compared to the specimen without a steel plate. The inclusion of a steel plate results in enhancement percentages of 24%, 40%, 46%, 37%, and 46% for V1, V2, V3, V111, and V12, respectively, as depicted in Figure 11. Some studies have utilized steel plates in two-way voided slabs to address punching shear occurring in slab areas near columns, and an increase in the ultimate load was observed with increasing steel plate thickness [3].

However, no studies have used steel plates in one-way slabs. The arrangement of plates within the slabs V111 and V12 did not gain a load capacity greater than that of the equivalent plate V3. In addition, the ultimate load of the V111 arrangement was lower than that of V12 due to using three steel plates in each rib. As a result, the number of holes increased, potentially leading to a decline in the overall strength of the steel plates. Overall, this finding reveals that the utilization of a steel plate significantly enhanced the structural integrity of voided slabs. Three factors related to the steel plates are principally responsible for the enhanced performance. First, the concrete confinement between them successfully prevented flexural bending cracks and diagonal shear cracks from forming and propagating. Second, the significant vertical forces generated by the steel plates resisted the applied load, thereby improving the inertial resistance of the samples. Third, the plates helped redistribute the load away from the heavily damaged area under the mid-span stub to less-stressed regions of the slab, which explains the existence of slight cracks near the supports. Lastly, during testing, a consistent type of failure was observed, characterized by the tension reinforcement bars giving way and then crushing the concrete. All specimens' failure mode was ductile flexural failure, followed by the concrete crushing at the slabs' top surface. The specimens strengthened with a steel plate have more ductile failure.

Table 4. Test results of specimens

Sy	Max load (KN)	Max def (mm)	Load at yield	Def at yield (mm)	Ductility	Toughness (KN.mm)	Stiffness (KN/mm)	First crack (KN)
S	60.00	14.10	55.20	11.02	1.28	702.00	5	12.8
V0	45.90	13.42	43.50	11.66	1.15	457.64	3.73	9.8
V1	56.70	30.67	50.90	12.44	2.47	1407.76	4.1	10.2
V2	64.40	25.65	57.90	12.46	2.06	1250.22	4.65	10.12
V3	67.20	23.08	60.20	12.01	1.92	1213.01	5	9.9
V111	62.70	25.99	56.80	12.30	2.11	1262.62	4.61	10.3
V12	66.90	23.25	61.00	13.22	1.76	1123.26	4.62	10.2

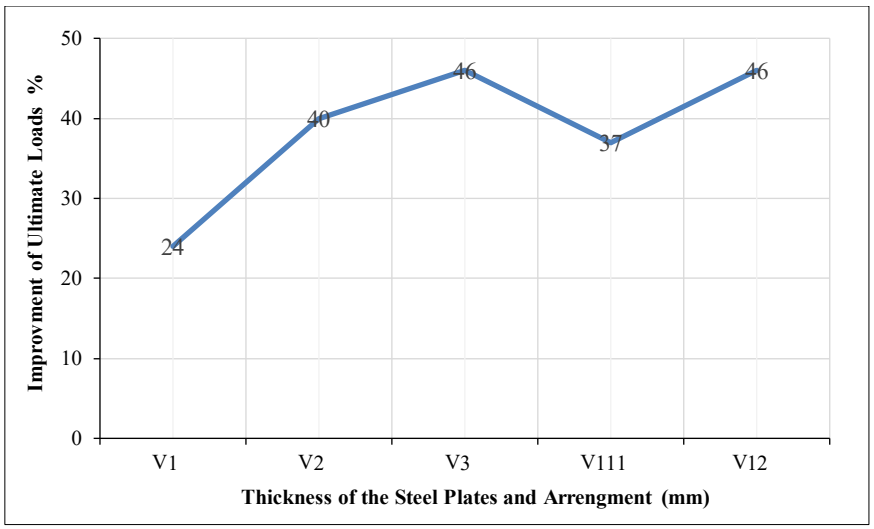

Figure 11. Percentage of enhancement with the presence of steel plates

3.2. Load-deflection Behavior

3.2.1. General Behavior

Table 4 presents the deflection at ultimate loads for all samples. Load-deflection responses at the slabs' midspan are depicted in Figure 12. The responses of the seven slabs were almost identical and comprised two phases: pre-yielding and post-yielding. Pre-cracking and post-cracking are included in the pre-yielding stage. The pre-cracking phase occurred from the beginning of the test until the first flexural fracture, during which the applied load and deflection increased gradually. The post-cracking phase, the second phase, continued until the tensile reinforcement yielded, at which point cracking, as expected, led to decreased stiffness.

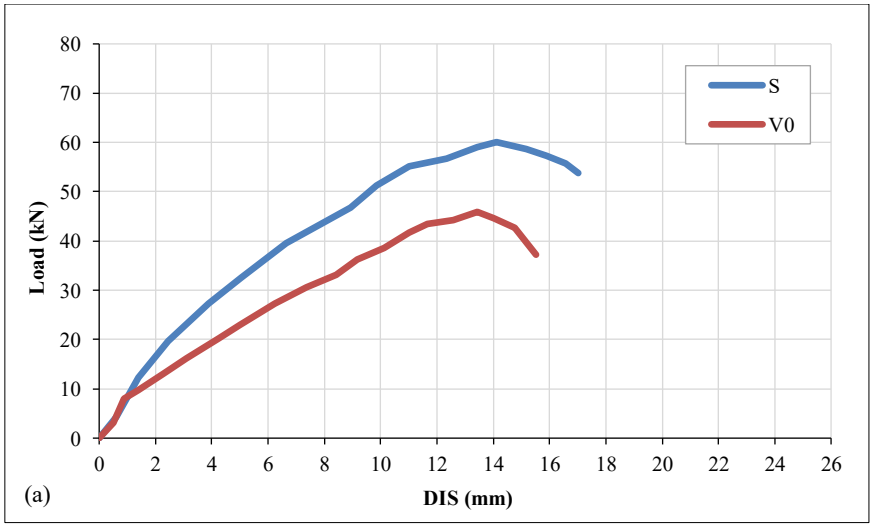

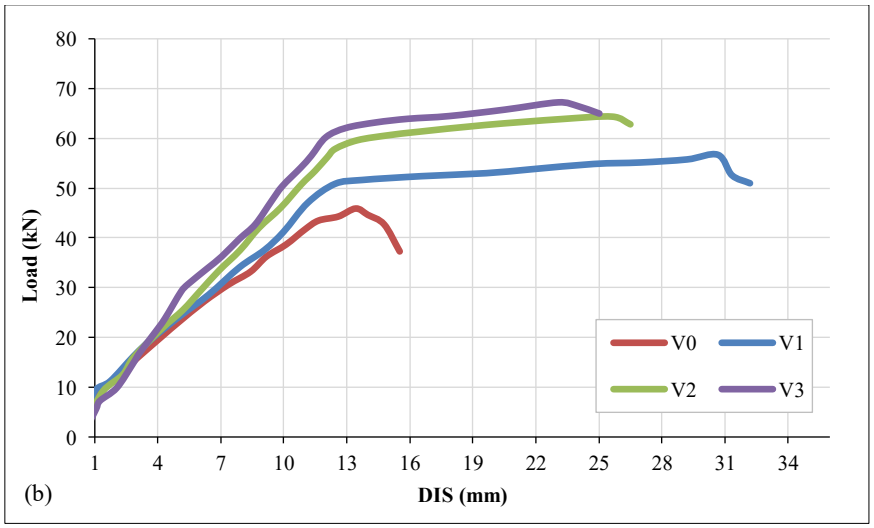

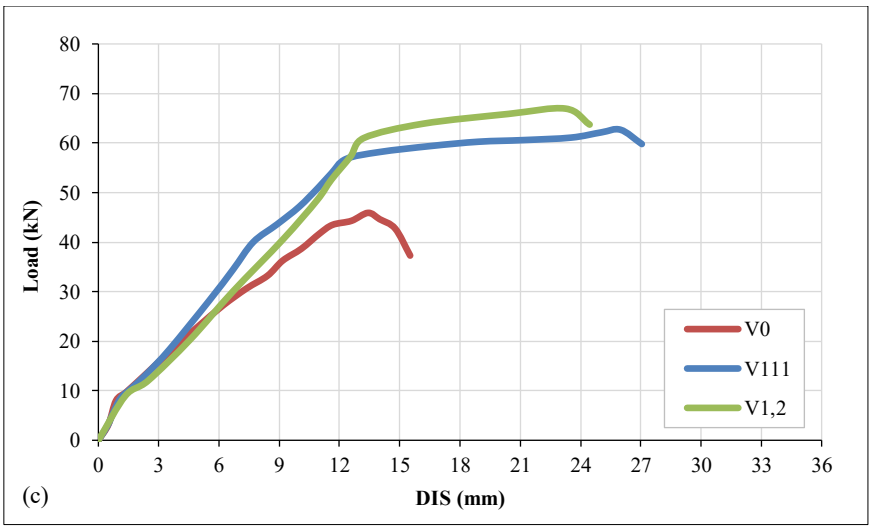

Figure 12. Applied load versus central displacement curves of all specimens (a) applied load versus central displacement curves of specimens (S, V0) (b) applied load versus central displacement curves of specimens (V0, V1, V2, V3) (c) applied load versus central displacement curves of specimens (V0, V1,1,1, V1,2).

The second stage, which is also called the plastic plateau or post-yielding, began when the tensile rebars yielded and continued until the specimen collapsed. At this phase, the deflection noticeably rises along with a slight increase in load. Previous studies reported similar responses [8, 27]. The ductility of the slabs was enhanced, particularly those strengthened with steel plates, due to a longer plastic plateau, or last stage, compared to the unstrengthened slabs (S, V0).

3.2.2. Deflection

The mid-span deflection of each slab was gauged during static testing. Figure 12 portrays load-displacement curves for all specimens. All seven specimens exhibited approximately identical deflection characteristics in their initial, pre-cracked stage. However, once cracking began, the rate of deflection accelerated noticeably. Figure 9-a depicts that the reference slab, labelled as S, demonstrated better load-bearing and deflection characteristics than the voided slab, V0, because of its uninterrupted and continuous structure. A comparison of the deflection between the voided specimen V0 and the solid specimen S at the service load stage (approximately 70-75% of the peak load of the solid specimen S, according to Tan and Zhao, 2004) was performed [28]. The findings indicate that the voided specimen V0 deflected approximately 57% more than that of the solid specimen S. This finding aligns with the outcomes documented in earlier studies [8, 26]. This indicates that the presence of voids decreases the slab's stiffness, due to the rapid extension and expansion of cracks in the voided area. It also highlights the negative effect of voids on structural performance.

Among the tested specimens, the strengthened specimens exhibited the stiffest behavior. At the same time, the voided slab lacking a steel plate (V0) displayed the softest load-deflection behavior, as illustrated in Figures 12-b and 12-c. Figure 12-b clearly illustrates that at the beginning, the displacement curves for V0, V1, V2, and V3 samples are identical. Subsequently, as the load increased and approached the ultimate load, they began to diverge. The deflection of the strengthened specimens (V1, V2, and V3) was examined at the service load of the voided slab (V0). These specimens achieved less deflection than the unstrengthened voided specimen by approximately 16%, 26%, and 32%, respectively. It was noted that the deflection decreased with increasing steel plate thickness. This reduction in deflection was also observed in a previous study [3] involving a two-way voided slab. These enhancements can be attributed to the steel plate effectively mitigating the negative influence of the voids on slab stiffness by restricting the growth and spread of shear and flexural cracks. Furthermore, the steel plate simultaneously served as reinforcement for shear and bending, thereby improving the effective moment of inertia of the specimens. This ultimately results in a higher yield and ultimate load capacity than a V0 slab without plates.

Figure 12-c compares the load-displacement curves for V0 and specimens with the arrangement of the steel plates. It was also observed that the specimens exhibited identical behavior at the beginning of the test. However, their curves began to diverge as the load rose toward the ultimate capacity. At the service load of V0, the deflection of the V111 and V12 was approximately 30% and 10% lower than that of V0, respectively. This indicates that the V12 arrangement exhibited greater improvement in flexural strength than the V111 slab. Moreover, the increased number of holes in the V111 slab potentially reduces the flexural strength of the plates and their yield and ultimate loads, as highlighted previously. Therefore, toughness and ductility were increased above the V12 slab.

At collapse, the deflection of V0 was about 13% lower than that of the solid slab S. The strengthened specimens, however, eventually had higher deflections than the solid specimen, reaching 45%, which decreased with the steel plate thickness. This outcome can be attributed to the enhanced ductility, toughness, and stiffness of these specimens, which resulted from reducing the negative influences of voids.

3.3. Stiffness

Table 4 demonstrates the stiffness of all specimens. It is structurally useful to assess the impact of steel plate thickness on the stiffness of the voided one-way specimens. Numerous methods for calculating an element's stiffness are presented in the literature, including yielding, secant, and service stiffness [29-31]. Flexural stiffness is the best method for the current investigation, as it considers the samples' initial slope of the load-deflection curve (post-yielding). The yielding force, Py, is divided by its corresponding displacement, Δy, to get the stiffness [32].

The voided specimen with no steel plate (V0) showed about 25.4% less stiffness than the solid slab when compared to the solid specimen (S). This result is consistent with previous research findings [8, 26]. The existence of voids is contributing to this, as it reduces the inertia moment of the voided slab. Also, it accelerated the expansion and development of cracks. Because voids were positioned directly above the tensile rebars, some of the surrounding concrete was removed, which reduced the bond strength. On the other hand, stiffness increases with an increase in plate thickness, as observed in Figure 13, thereby improving bending strength. This increase in stiffness is mainly due to the steel's higher modulus of elasticity than concrete; The steel plate effectively acts as a layer of reinforcement in the tension zone. This addition effectively compensates for the reduction in stiffness caused by the internal voids, simultaneously restricting crack propagation and maintaining the structural integrity of the bond region, particularly of the V3 specimen, which exhibited stiffness close to that of the solid specimen. The arrangement in the V111 and V12 slabs demonstrated nearly identical results.

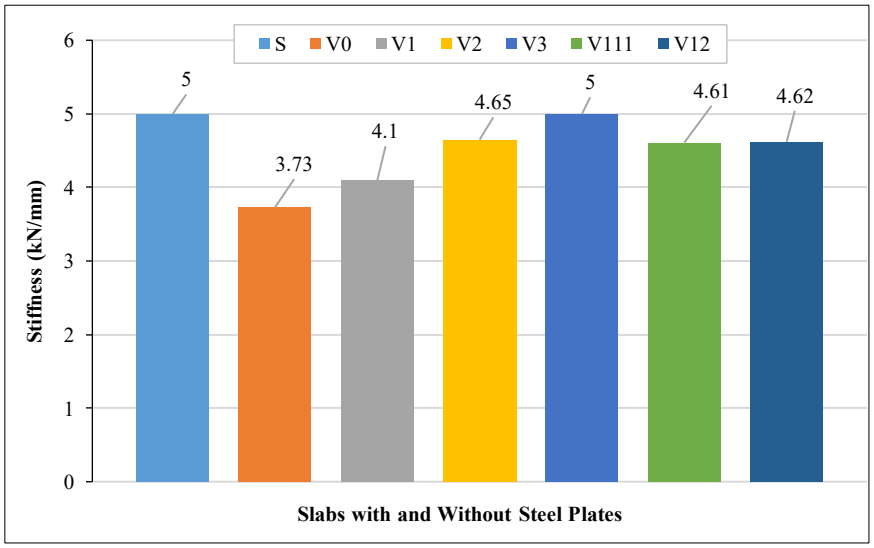

Figure 13. Stiffness for all slabs

3.4. Ductility

Ductility is the structural component's ability to tolerate significant inelastic deformation before breaking [33, 34]. To protect people and their belongings and to provide sufficient notice before failure, the ductility of RC components should be carefully considered throughout their design. Consequently, assessing the effect of voids on the slabs' ductility is required. The ductility was computed as the ratio (Δu/Δy), where Δu and Δy represent the displacements at the ultimate and yield loads, respectively.

Table 4 and Figure 14 present the findings. The ductility value was lowered by approximately 10% on the V0 specimen in comparison with the solid specimen S. Nevertheless, it was revealed that the ductility index improved when steel plates were used to reinforce the voided slabs. The plate helps the internal rebars more effectively enter the yielding range by maintaining the voided portion intact under high strain for a longer period. It was also observed that ductility improvement decreased as plate thickness increased, as the plates provided additional flexural reinforcement. However, the trend of a declining ductility index with increasing plate thickness (V1–V3) is consistent with the behavior of heavily reinforced members. The failure mode shifts from one dominated by tension bar yielding (ductile) to one characterized by a larger un-cracked section and delayed yielding of the main reinforcement as the steel plate thickness increases, with its contribution to the ultimate moment increasing dramatically. Notably, the failure mode for all strengthened specimens remained the same: ductile flexural failure, despite the quantitative decrease in the ductility index. This demonstrates

that, even in the stiffer portion, the steel plate effectively prevented a transition to a brittle failure mechanism, guaranteeing structural integrity and providing a warning of impending collapse. The ductility improvements for the V1, V2, V3, V111, and V12 specimens were 114%, 79%, 66%, 83%, and 53% compared to the V0 slab and 92%, 61%, 50%, 65%, and 38% compared to the solid specimens S due to the lengthened plastic plateau or last stage compared to the unstrengthened slabs (S, V0). These findings were also observed in a previous study [3] involving a two-way voided slab. V111 slab's arrangement demonstrated greater ductility than the V12 slab as it yielded at a lower load.

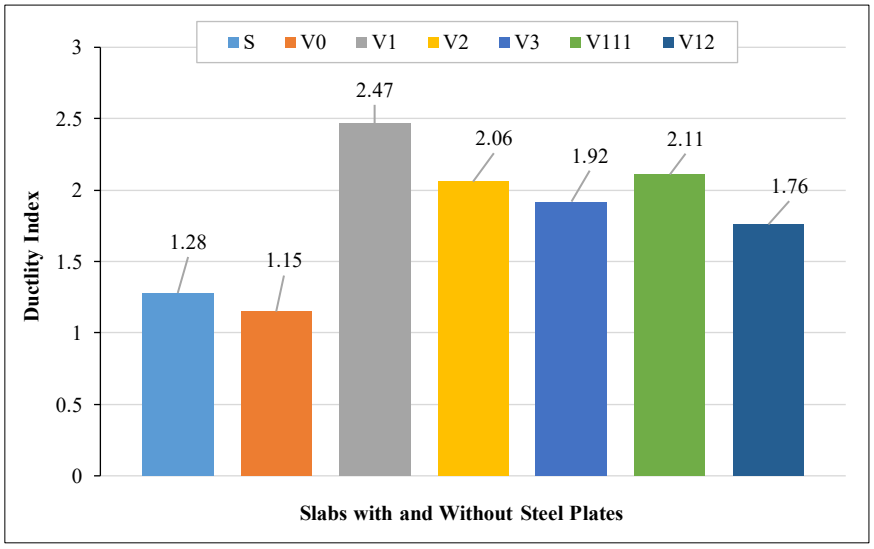

Figure 14. Ductility for all slabs

3.5. Toughness

Toughness refers to the region beneath the load-deflection curve. It describes the amount of energy absorbed by structural elements before collapse [33, 35]. Table 4 illustrates the toughness values for all specimens. Additionally, Figure 15 illustrates these values. The outcomes reveal that the voided specimen's V0 demonstrated a notable 35% loss in toughness relative to the solid slab S.

Figure 15. Toughness for all slabs

The energy absorption in the concrete members is precisely correlated with the concrete's resistance to fracture and cracking. Since voids account for a large percentage of the concrete, the voided slabs' ability to absorb energy is reduced. On the other hand, adding steel plates to the voided slab had a greater impact on energy absorption because their activation delayed concrete fracture and slowed the spread of cracks. The absorption of energy of the V1, V2, V3, V111, and V12 were 207.6%, 173.2%, 165%, 176%, and 145%, respectively, compared to the V0, and 100.5%, 78%, 73%, 78%, and 60% in comparison with the solid specimens S. These findings were also observed in a previous study [3] involving a two-way voided slab. This increase is primarily attributed to the steel plate's ability to restore stiffness and extend the plastic deformation phase. It is noted that toughness decreased with increasing steel thickness due to increased

strength and reduced plastic deformation. The V1 sample, in particular, achieves superior toughness comparable to the solid reference slab S (100.5%), due to an increase in the area under the curve resulting from greater plastic deformation at complete failure. The higher toughness of V111 over V12 is due to its greater overall deformation capacity before failure

3.6. Reinforcing Bar Strains

Figure 16 illustrates the load-steel strain curves of the tension bar longitudinal reinforcement at the center of the central bar, as previously mentioned. Notably, none of the slabs reached the yield strain at the service load, which is 70% of the solid slab's peak load. The unstrengthened voided slab V0 exhibited the most strain among the tested specimens. The adopted service load for this slab was nearly 92% of its failure load. Figure 16-a compares the Load-steel strain curves of S and V0 specimens, when compared at the service stage (0.7 times that of S). The results demonstrated that the V0 specimen experienced a strain of approximately 61% more than the reference slab S. This indicates that the fractures penetrated further through the thickness of the slab, causing the neutral axis to shift closer to the top surface. This shift diminished the slab's load-bearing capacity, reduced its flexural stiffness, and altered its structural behavior, leading to higher strain. Similarly, Figure 16-b compares the Load-steel strain curves of V0, V1, V2, and V3. At the service stage of the unstrengthened specimen V0, the strengthened voided slabs V1, V2, and V3 exhibited strains that were lower than those of the voided slab without a steel plate by about 26%, 35%, and 38%, respectively. Figure 16-c presents that the V111 and V12 arrangement specimens exhibited a 39% and 40% decrease in strain compared to the strain at the service stage of the V0 specimen. These results demonstrate that the steel plates served as effective longitudinal reinforcement. At ultimate loads, each specimen demonstrated a measured strain exceeding the yield strain of the tension steel bar, 2500 macrostrains. The recorded strain values increased by approximately 10%, 248%, 98%, 128.6%, 183.6%, and 69% for V0, V1, V2, V3, V111, and V12, respectively, relative to the solid slab S. The use of steel plates for strengthening improves the specimens' structural performance by increasing their capacity to support loads and enabling the redistribution of strain. This results in a greater load-bearing capacity and overall performance when compared to unstrengthened V0 specimens.

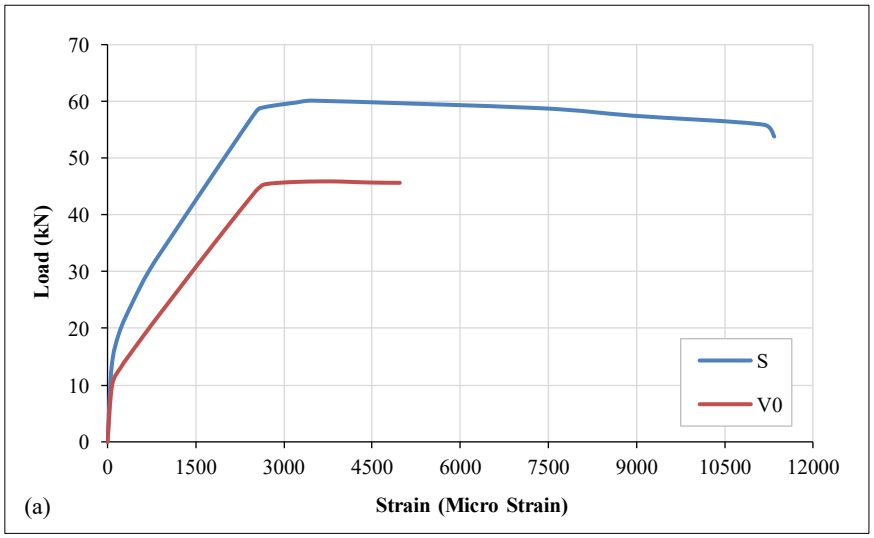

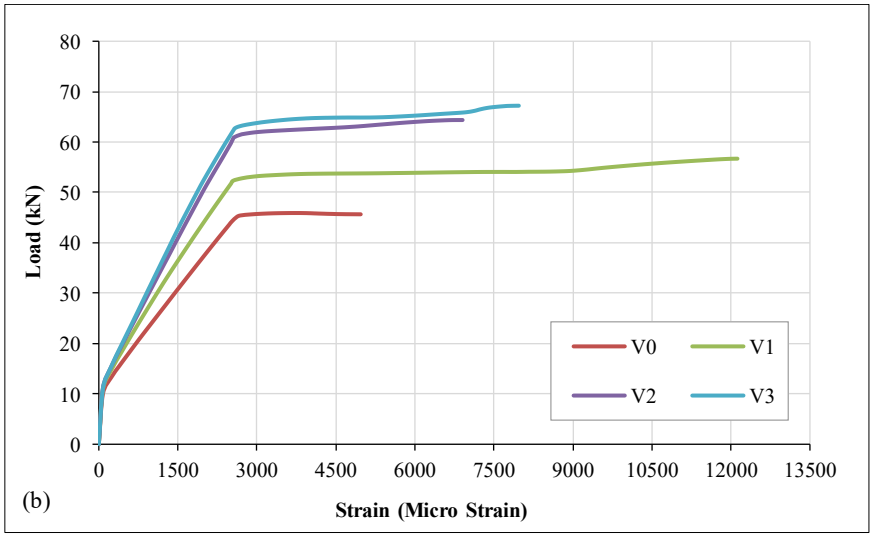

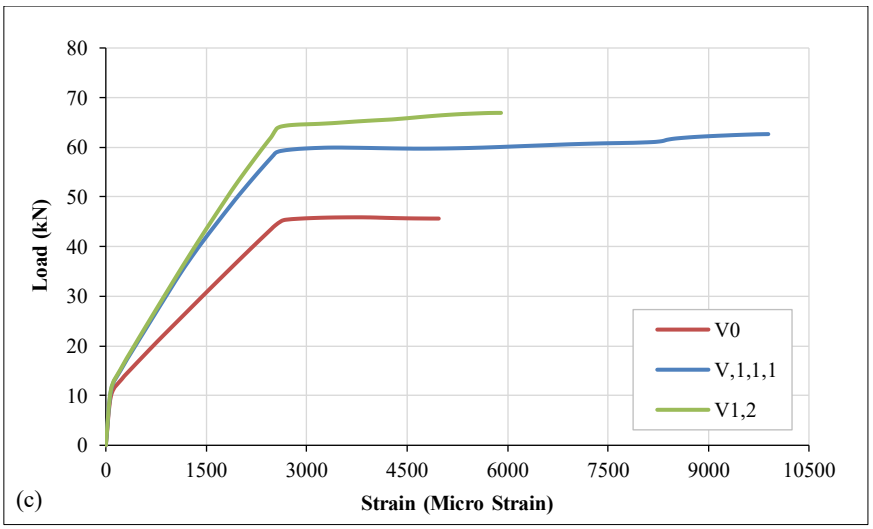

Figure 16. Load-steel strain curves (a) load-steel strain curves of S and V0 specimens (b) load-steel strain curve of V0, V1, V2, and V3 specimens (c) load-steel strain curve of V0, V111, and V12 specimens

Generally, the results reflected that the V12 arrangement specimen exhibited the optimum behavior. Its maximum strain at collapse was lower than that of the other specimens, and it demonstrated increased bearing capacity and minimal deformation. This performance is attributed to the specific plate arrangement, which significantly enhanced its flexural strength and moment of inertia. In contrast, the V111 specimen demonstrated greater deformation and lower load capacity than the V12 specimen due to a reduction in its flexural strength. This difference can be attributed to the increased number of holes in the V111 arrangement, as previously mentioned. These arrangements led to a demonstrable increase in both the ductility and toughness of the reinforced voided slab.

3.7. Steel Plate Strains

The strain on the steel plates was measured at three points: at the midpoint of each plate, directly under the point load, and 350 mm from the support (see Figure 6). Figures 17 and 18 indicate that the steel plates remained in the elastic state under service loads, except for the one mm-thick plate. The early yield observed in the 1 mm steel plate explains why the V1 slab exhibited greater ductility and toughness than the other specimens. The strains increased at the center of the plates, indicating that the flexural cracks passed through this point and that the elevated stresses were immediately transferred to the plates. Conversely, the strains decreased at the other two locations, as illustrated in Figures 18 and 19. At the location 350 mm away from the support, none of the slabs reached yield strain at both service and ultimate load because the concrete retained the ability to support a portion of the applied load in these regions, as presented in Figure 19. At the ultimate loads, the strain in the plates at the center and directly beneath the point load fundamentally changed and reached a plastic state. The plates' ability to achieve the yield strain suggested they were tightly bonded to the slabs. In general, comparing strain at the two load levels (service and ultimate) demonstrates that the effect of the steel plates on strengthening the RC voided slabs became more apparent as cracks widened. Overall, the steel plates had the greatest influence on the voided specimens, particularly in V3 and V12, which demonstrated greater load-carrying capacity and less deformation than the reference slab.

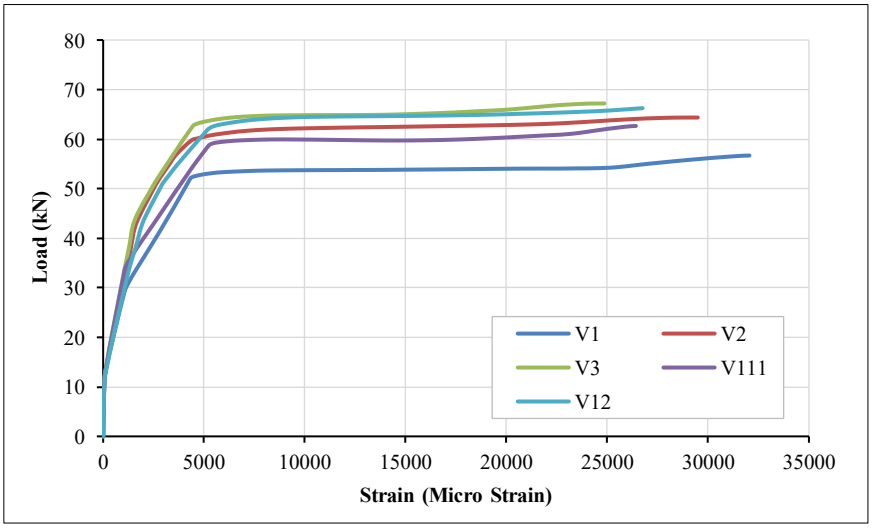

Figure 17. Load-strain curves at the midspan of steel plates

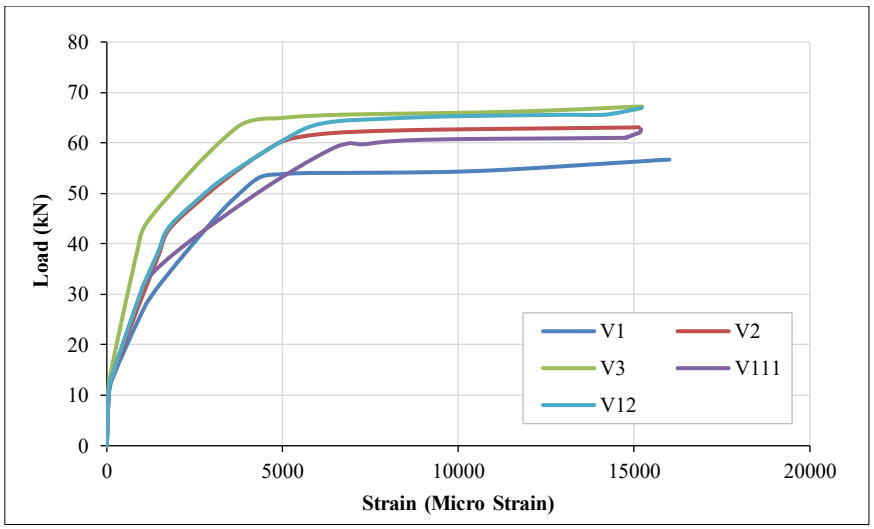

Figure 18. Load-strain curves of steel plates under a point load

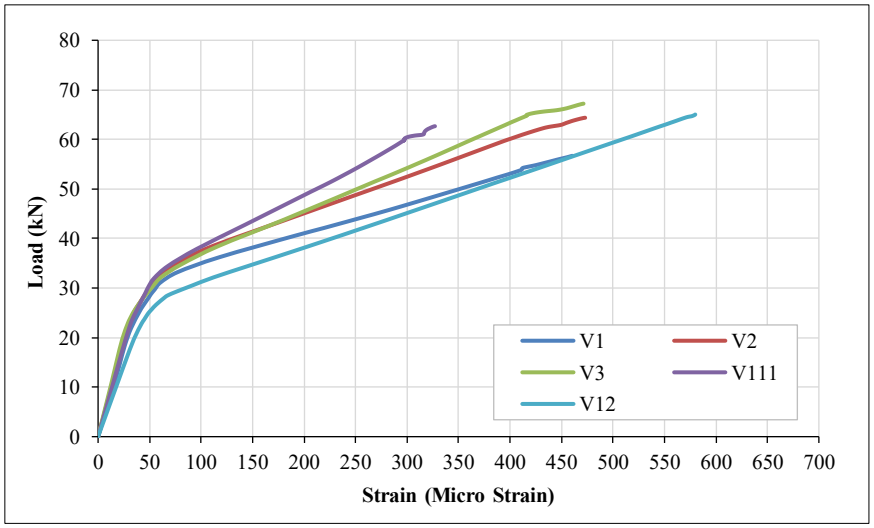

Figure 19. Load-strain curves of steel plates at 350 mm from the support

4. Numerical Study

4.1. Finite Element Model (FEM)

The ABAQUS Finite Element (FE) software version (2019) was used to analyze three-dimensional numerical models of slabs. In this modelling, RC slabs were modeled using three-dimensional 8-node linear brick solid elements (C3D8R) and the steel reinforcing was simulated using three-dimensional 2-node truss elements (T3D2), whereas the steel plate was modeled using shell elements with four nodes and reduced integration (S4R). It was assumed that the concrete and the steel bars and plates would bond perfectly. The perfect bond was assumed to be based on

- The plates were extended along the length of the specimens, and as a result, the required development length was achieved.
- Their length was perforated, and it was demonstrated that this method of connection was effective in Lameiras et al. [25].
- They were positioned directly between the top and bottom steel meshes, which caused friction forces to develop between the plate edges and rebar ribs. Additionally, the plates reached the yield strain, which supports this assumption.

The Concrete Damage Plasticity Model (CDPM) was utilized to model the concrete failure: compressive crushing and tensile cracking [36]. The CDPM was given stress-strain values in compression and tension, depending on the concrete's test compressive strength, using the standard formulas from Hu & Schnobrich [37]. Additionally, the Zhang et al formula [38] was used to introduce the softening portion of the stress-strain curve of concrete in tension, which represents the interaction between the concrete and the steel bars. The steel bars and steel plates were modeled as an elastic-perfectly plastic material.

4.2. Validation of the Adopted Model

The agreement between the numerical load-deflection curve and experimental results is considered a critical aspect for validating the Finite Element Model (FEM), as this curve encompasses response parameters such as ultimate load, maximum deflection, ductility, stiffness, energy absorption, and yield [3]. To accomplish this, the mesh size and two of the five CDPM parameters, including dilation angle and viscosity, were thoroughly examined. After several trials, it was discovered that the mesh size of 20 mm produced a reasonably accurate result. The dilation angle and viscosity for slabs have been determined to be 31° and 0.0001, respectively. The default values for the remaining parameters of CDPM, which are stress ratio, eccentricity, and shape factor, were chosen as 1.16, 0.1, and 0.67, respectively. Figure 20 compares the numerical load-deflection responses with the experimental results for the seven specimens, and the validation results are deemed satisfactory. Boundary conditions were simulated to resemble those identified in experimental conditions. The ends of the slabs were supported by simple supports, which were modeled as elastic supports. One support permitted rotations about the x-axis but restricted longitudinal and vertical displacements (in the y and z directions) (a pinned support). The second support allowed rotations about the x-axis and longitudinal displacements (a roller support). However, it only permitted limited vertical displacements (in the y-direction). A flexural load test was performed on the models. Figure 20 compares the load-deflection results of the seven specimens' tests with those from the FE analysis. There is a satisfactory level of agreement between the test and FE analysis results. The predicted analytical and experimental ultimate load ranges from 1.00 to 1.13, as listed in Table 5.

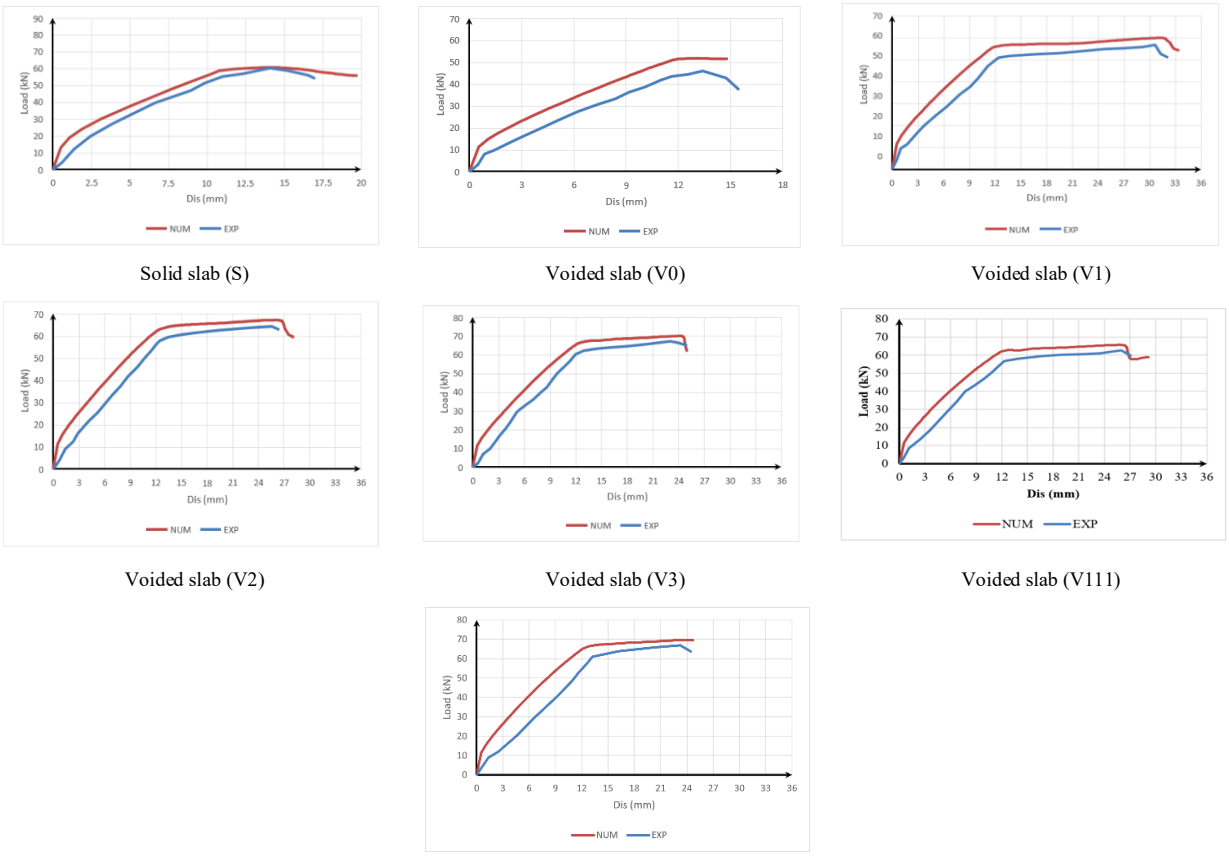

Figure 20. FEM & EXP. Load-displacement curves of seven specimens

Table 5. Test results of specimens

Specimens	Experimental ultimate load (kN)	Analytical ultimate load, ABQUAS (kN)	P_{FE}/P_{test}
S	600.00	60.44	1.00
V0	45.90	51.82	1.13
V1	56.70	59.7	1.05
V2	64.40	67	1.05
V3	67.20	69.91	1.04
V111	62.70	65.70	1.05
V12	66.90	69.55	1.04

4.3. Damage of the Analyzed Slabs

The crack initiation and propagation patterns observed in the FEM were comparable to those seen in the experimental investigation. Figure 21 illustrates that the crack patterns from the FE and experimental investigations were quite similar, indicating that the proposed FE model accurately captured the behavior of slab specimens at failure loads. According to CDPM, cracking occurs when a point's tensile equivalent Plastic Strain Magnitude (PEMAG) is more than zero [39], as depicted in Figure 21. It was observed that the maximum plastic strain was highest in the unstrengthened specimen V0, indicating that cracks widened faster due to the voids. However, when steel plates were used, the plastic strain values decreased, indicating that the steel plates were superior in preventing the crack from growing and widening. Their effectiveness became even more impressive after the first crack started.

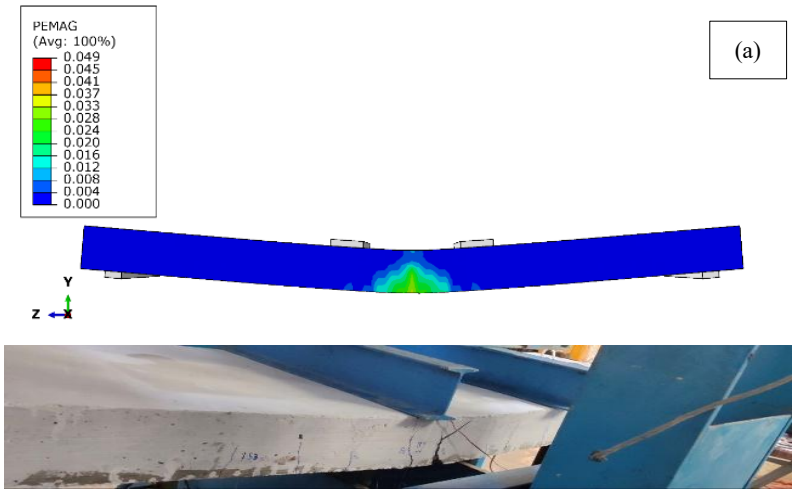

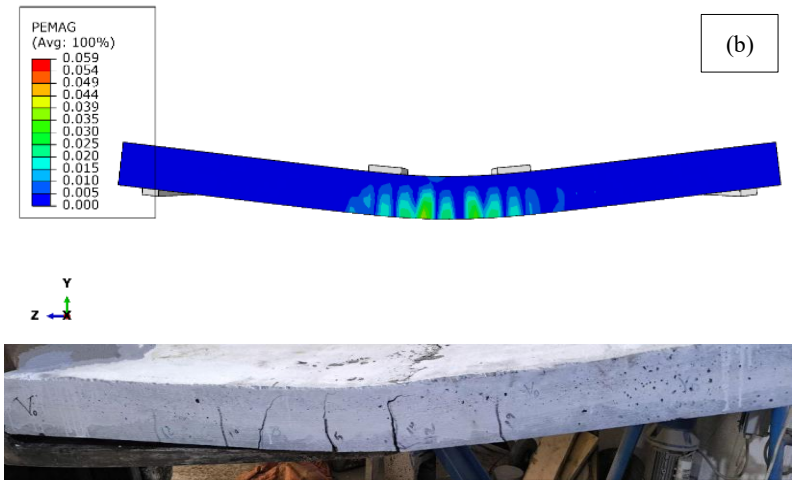

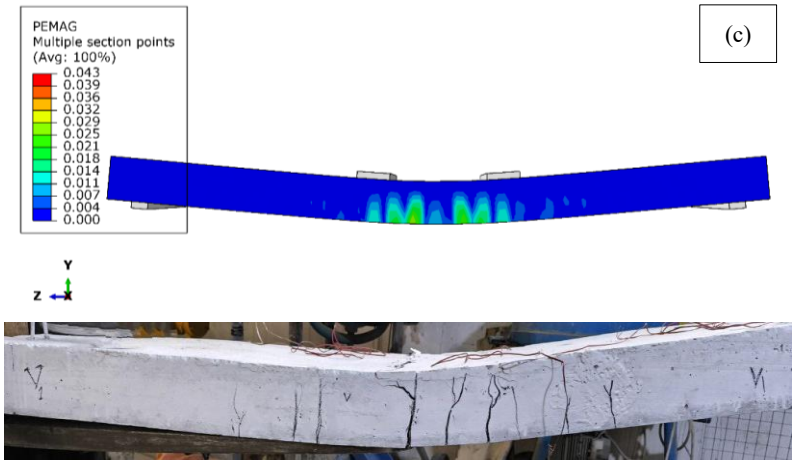

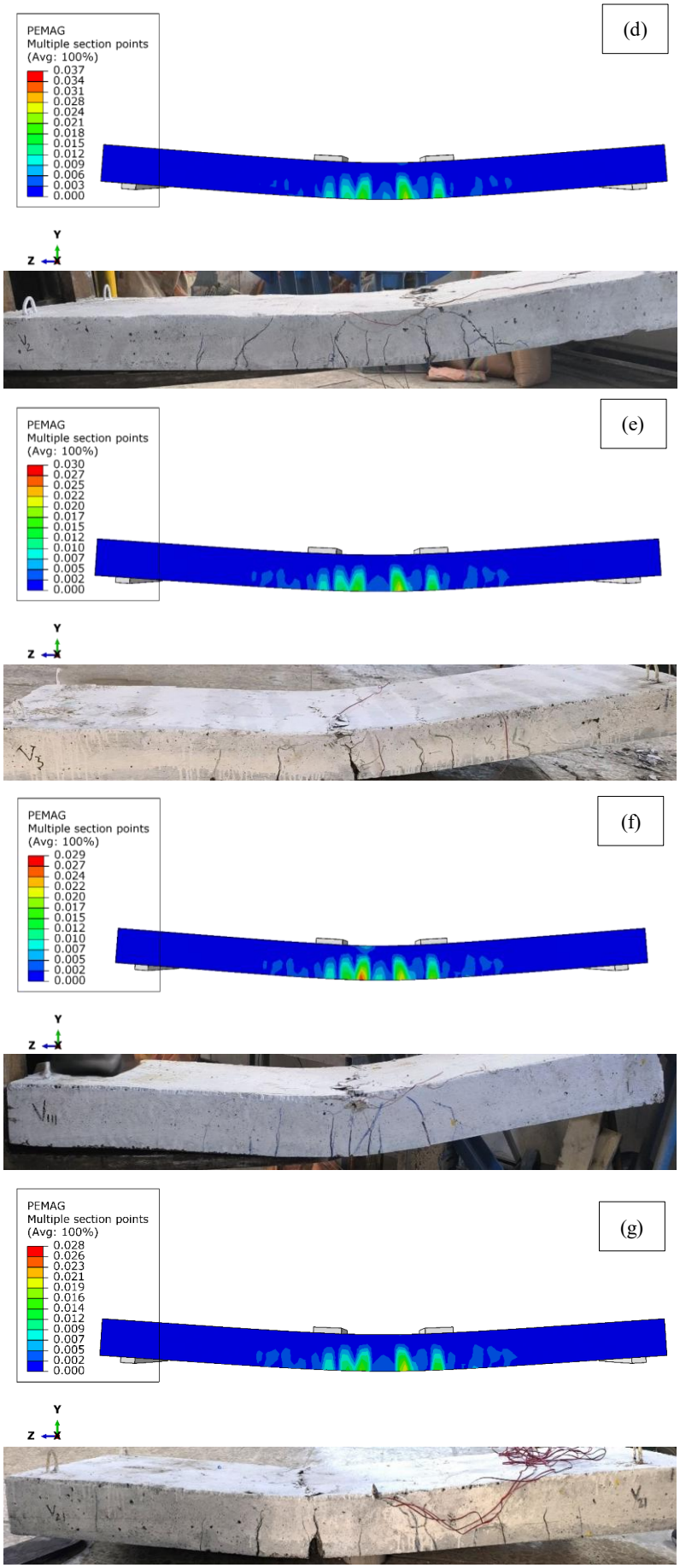

Figure 21. FEM & EXP crack patterns (a) solid specimen S (b) voided specimen V0 (c) voided specimen V1 (d) voided specimen V2 (e) voided specimen V3 (f) voided specimen V111 (g) voided specimen V12

5. Conclusions

This study proposed a novel, easy way to improve the behavior and strength of one-way voided slabs by embedding steel plates within RC voided slabs. As part of the experimental program, seven specimens were fabricated and subjected to static force testing until failure. One slab had a solid cross-section, while the other six were voided by gradually spreading 27 cuboid voids throughout them. Five of them were reinforced with steel plates that were 1, 2, and 3 mm thick, and one was not. Furthermore, the experimental results were validated through FE analysis. The following are key findings from the FE and experimental data:

- The failure mode for all specimens was flexural, and the utilization of steel plates successfully rendered the flexural failure more ductile.
- The presence of voids increases stress concentrations in the thin areas of the flange and ribs around the voids, leading to fractures that penetrate deeper into the slab's thickness, reducing the overall performance of the voided slab, and crushing the top face of the specimens.
- The study reveals a proportional relationship between the slab's strength, mid-span displacement, stiffness, tension bar strain, steel plate strain, and the thickness of the reinforced steel plate.
- The strength of the voided slab V0 was reduced by 23.5% compared with the solid specimen S. Conversely, using steel plates increased the ultimate loads and improved ductility and toughness by 114% and 207.6%, respectively, compared with the V0 sample.
- The increase in strain of the tension bar for specimens without reinforcement, V0, was 10%, compared to the control specimen S. For samples reinforced with a steel plate, the increase ranged from 69% to 248%, relative to the solid slab S.
- At the service stage of the solid slab, the increase in displacement due to the existence of voids was 57% for V0. In comparison, reinforcement with steel plates of 1 mm, 2 mm, and 3 mm thicknesses resulted in decreased deflection, with values of 16% for V1, 26% for V2, 32% for V3, 30% for V111, and 10% for V12.
- In specimen V0, which lacked a steel plate, the number of cracks decreased, while the cracks widened and became concentrated in the specimen's middle span.
- The spread of cracks across the specimens' width indicates that the steel plates successfully distributed the stress throughout the specimens. Additionally, it provides increased flexural reinforcement strength, whereby deflection decreases as the steel plate thickness increases. It also helped delay the onset of the first crack by bearing a portion of the applied load.
- Sample V1 exhibited the greatest deflection because it yielded at the minimum load among the other samples, with the greatest strain at failure load, measuring roughly 12123.7 mm and 32050.9 mm in the center of the steel plate and rebar, respectively. This produced the highest levels of toughness and ductility among the examples.
- The parametric study revealed that the activation of steel plates increased with increasing thickness. Therefore, V3 sustained the maximum load-bearing capacity and stiffness among the specimens, which was equal to the stiffness of solid specimens.
- The steel plate placement in specimen V12 demonstrated better performance than in V111 in terms of strength and deflection. However, the latter specimen exhibited the highest ductility and toughness. This arrangement is more advantageous in seismic regions.
- The effectiveness of the steel sheets in preventing the development and spread of cracks was confirmed by FE analysis. Additionally, they have been observed to function as both shear and flexural reinforcements at the same time.

6. Declarations

6.1. Author Contributions

Conceptualization, F.H.A. and H.A.J.; methodology, F.H.A.; software, F.H.A.; validation, F.H.A., H.A.J., and Z.Z.; formal analysis, F.H.A.; investigation, F.H.A.; resources, F.H.A.; data curation, F.H.A.; writing—original draft preparation, F.H.A.; writing—review and editing, F.H.A.; visualization, F.H.A.; supervision, F.H.A.; project administration, F.H.A.; funding acquisition, H.A.J. All authors have read and agreed to the published version of the manuscript.

6.2. Data Availability Statement

The data presented in this study are available on request from the corresponding author.

6.3. Funding

The authors received no financial support for the research, authorship, and/or publication of this article.

6.4. Conflicts of Interest

The authors declare no conflict of interest.

7. References

[1] Valivonis, J., Jonaitis, B., Zavalis, R., Skuturna, T., & Šneideris, A. (2014). Flexural capacity and stiffness of monolithic biaxial hollow slabs. Journal of Civil Engineering and Management, 20(5), 693–701. doi:10.3846/13923730.2014.917122.

[2] Oukaili, N., Merie, H., Allawi, A., & Wardeh, G. (2024). Reduced Volume Approach to Evaluate Biaxial Bubbled Slabs' Resistance to Punching Shear. Buildings, 14(3), 676. doi:10.3390/buildings14030676.

[3] Al-Gasham, T. S., Mhalhal, J. M., & Jabir, H. A. (2019). Improving punching behavior of interior voided slab-column connections using steel sheets. Engineering Structures, 199, 109614. doi:10.1016/j.engstruct.2019.109614.

[4] Abishek, V., & Iyappan, G. R. (2021). Study on flexural behavior of bubble deck slab strengthened with FRP. Journal of Physics: Conference Series, 2040(1), 12018. doi:10.1088/1742-6596/2040/1/012018.

[5] Jabir, H. A., Mhalhal, J. M., & Al-Gasham, T. S. (2021). Conventional and bubbled slab strips under limited repeated loads: A comparative experimental study. Case Studies in Construction Materials, 14, 501. doi:10.1016/j.cscm.2021.e00501.

[6] Ibrahim, A. M., Ismael, M. A., & Abdul Hussein, H. A. S. (2019). the Effect of Balls Shapes and Spacing on Structural Behaviour of Reinforced Concrete Bubbled Slabs. Journal of Engineering and Sustainable Development, 23(2), 56–65. doi:10.31272/jeasd.23.2.5.

[7] Sagadevan, R., & Rao, B. N. (2019). Effect of void former shapes on one-way flexural behaviour of biaxial hollow slabs. International Journal of Advanced Structural Engineering, 11(3), 297–307. doi:10.1007/s40091-019-0231-7.

[8] Al-Gasham, T. S., Hilo, A. N., & Alawsi, M. A. (2019). Structural behavior of reinforced concrete one-way slabs voided by polystyrene balls. Case Studies in Construction Materials, 11, 292. doi:10.1016/j.cscm.2019.e00292.

[9] Ibrahim, A. M., Ismael, M. A., & Hussein, H. A. A. (2019). . (2019). Effect of Construction Type on Structural Behaviour of R.C Bubbled One-Way Slab. Diyala Journal of Engineering Sciences, 12(1), 73–79. doi:10.24237/djes.2019.12109.

[10] Saleh, Y. A., Abdulla, A. I., & Jomaa'h, M. M. (2025). Flexural behavior of one-way voided reinforced concrete slabs under the influence of uniformly distributed static loads. Journal of Advanced Sciences and Engineering Technologies, 8(1). doi:10.32441/jaset.8.1.1.

[11] Al-Ahmed, A. H. A., Ibrahim, F. H., Allawi, A. A., & El-Zohairy, A. (2022). Behavior of One-Way Reinforced Concrete Slabs with Polystyrene Embedded Arched Blocks. Buildings, 12(3), 331. doi:10.3390/buildings12030331.

[12] Nareshnayak, N., & Rao, B. N. (2022). Numerical Analysis of One-Way Flexural Strength of Voided Slab. Structural Integrity, 27, 250–256. doi:10.1007/978-3-031-04793-0_19.

[13] Zavalis, M., Daugevičius, M., Jokūbaitis, A., Zavalis, R., & Valivonis, J. (2022). Deflection Estimation Model for Prestressed Concrete Slabs with Plastic Inserts Forming Voids. Materials, 15(9), 3013. doi:10.3390/ma15093013.

[14] Kıpçak, F., Erdil, B., Tapan, M., & Karaşin, A. (2023). The Effect of Voids on Flexural Capacity of Reinforced Concrete Slabs. Periodica Polytechnica Civil Engineering, 67(4), 1048–1065. doi:10.3311/PPci.21988.

[15] Golham, M. A., & Al-Ahmed, A. H. A. (2024). Strengthening of GFRP Reinforced Concrete Slabs with Openings. Journal of Engineering, 30(01), 157–172. doi:10.31026/j.eng.2024.01.10.

[16] Kareem, H. M., & Lateef, A. M. (2025). Flexural Behavior of Steel and GFRP-Reinforced Lightweight Concrete Hollow One-Way Slabs Under High Temperatures. Kufa Journal of Engineering, 16(4), 268–287. doi:10.30572/2018/KJE/160416.

[17] jamal, J., & Vijayan, V. (2020). A Study on Strengthening of Bubble Deck Slab With Elliptical Balls by Using GFRP Sheets. SSRN Electronic Journal. doi:10.2139/ssrn.3591289.

[18] Aman, S. S., Mohammed, B. S., Wahab, M. A., & Anwar, A. (2020). Performance of reinforced concrete slab with opening strengthened using CFRP. Fibers, 8(4), 25. doi:10.3390/fib8040025.

[19] Waryosh, W. A., & Hashim, H. H. (2020). Rehabilitation of Fire Damage Reinforced Concrete Bubbled Slabs. Www.Gsjpublications.Com Journal of Global Scientific Research, 1, 278–288.

[20] Abdulkhaliq, M., & Al-Ahmed, A. H. (2024). The Flexural Behavior of One-Way Concrete Bubbled Slabs Reinforced by GFRP-Bars with Embedded Steel I-Sections. Engineering, Technology & Applied Science Research, 14(4), 15860–15870. doi:10.48084/etasr.7680.

[21] Yaagoob, A. H., & Harba, I. S. (2020). Behavior of Self Compacting Reinforced Concrete One Way Bubble Deck Slab. Al-Nahrain Journal for Engineering Sciences, 23(1), 1–11. doi:10.29194/njes.23010001.

[22] Al-Azzawi, A. A., Abdulsattar, R., & Al-Shaarbaf, I. (2018). A state of the art review on reactive powder concrete slabs. International Journal of Applied Engineering Research, 13(1), 761-768.

[23] Alfeehan, A. A., Abdulkareem, H. I., & Mutashar, S. H. (2017). Flexural behavior of sustainable reactive powder concrete bubbled slab flooring elements. Challenge Journal of Structural Mechanics, 3(2), 81. doi:10.20528/cjsmec.2017.04.010.

[24] Ismael, B. H., Ali, Z. M., Hama, S. M., Aljumaily, M. M., Alshami, A. W., & Mohammed, S. S. (2025). Flexural Characteristics of Hollow One Way-Ferrocement Slabs. Engineering, Technology & Applied Science Research, 15(2), 22226–22231. doi:10.48084/etasr.10283.

[25] Lameiras, R., Valente, I. B., Barros, J. A. O., Azenha, M., & Gonçalves, C. (2018). Pull-out behaviour of Glass-Fibre Reinforced Polymer perforated plate connectors embedded in concrete. Part I: Experimental program. Construction and Building Materials, 162, 155–169. doi:10.1016/j.conbuildmat.2018.02.141.

[26] Vrcelj, Z., & Bradford, M. A. (2007). Elastic bubble augmented spline finite strip method in analysis of continuous composite beams. Australian Journal of Structural Engineering, 7(2), 75-84. doi:10.1080/13287982.2007.11464966.

[27] Schnellenbach-Held, M., & Pfeffer, K. (2002). Punching behavior of biaxial hollow slabs. Cement and Concrete Composites, 24(6), 551–556. doi:10.1016/S0958-9465(01)00071-3.

[28] Tan, K. H., & Zhao, H. (2004). Strengthening of Openings in One-Way Reinforced-Concrete Slabs Using Carbon Fiber-Reinforced Polymer Systems. Journal of Composites for Construction, 8(5), 393–402. doi:10.1061/(asce)1090-0268(2004)8:5(393).

[29] Jabir, H. A., Mhalhal, J. M., Al-Gasham, T. S., & Abid, S. R. (2020). Mechanical characteristics of deep beams considering variable a/d ratios: An experimental investigation. IOP Conference Series: Materials Science and Engineering, 988(1), 12030. doi:10.1088/1757-899X/988/1/012030.

[30] Abbass, A. A., Abid, S. R., Arna'ot, F. H., Al-Ameri, R. A., & Özakça, M. (2020). Flexural response of hollow high strength concrete beams considering different size reductions. Structures, 23, 69–86. doi:10.1016/j.istruc.2019.10.001.

[31] Al-Gasham, T. S., Mhalhal, J. M., & Abid, S. R. (2020). Flexural Behavior of Laced Reinforced Concrete Moderately Deep Beams. Case Studies in Construction Materials, 13, 363. doi:10.1016/j.cscm.2020.e00363.

[32] Malm, R. (2006). Shear cracks in concrete structures subjected to in-plane stresses. Ph.D. Thesis, KTH Royal Institute of Technology, Stockholm, Sweden.

[33] Abbass, A., Abid, S., & Özakça, M. (2019). Experimental investigation on the effect of steel fibers on the flexural behavior and ductility of high-strength concrete hollow beams. Advances in Civil Engineering, 2019, 8390345. doi:10.1155/2019/8390345.

[34] Ali Al-Tameemi, S. K., Al-Hasany, E. G., Mohammad, H. K., Jabir, H. A., Ibrahim, T. H., Allawi, A. A., & El-Zohairy, A. (2024). Simulation and design model for reinforced concrete slabs with lacing systems. Advances in Structural Engineering, 27(5), 871–892. doi:10.1177/13694332241237576.

[35] Mertol, H. C., Baran, E., & Bello, H. J. (2015). Flexural behavior of lightly and heavily reinforced steel fiber concrete beams. Construction and Building Materials, 98, 185–193. doi:10.1016/j.conbuildmat.2015.08.032.

[36] Kmiecik, P., & Kamiński, M. (2011). Modelling of reinforced concrete structures and composite structures with concrete strength degradation taken into consideration. Archives of Civil and Mechanical Engineering, 11(3), 623–636. doi:10.1016/s1644-9665(12)60105-8.

[37] Hu, H.-T., & Schnobrich, W. C. (1991). Nonlinear finite element analysis of reinforced concrete plates and shells under monotonic loading. Computers & Structures, 38(5–6), 637–651. doi:10.1016/0045-7949(91)90015-e.

[38] Zhang, Y. G., Lu, M. W., & Hwang, K. C. (1993). Nonlinear finite element analysis of concrete structures. ZAMP Zeitschrift Für Angewandte Mathematik Und Physik, 44(3), 537–555. doi:10.1007/BF00953666.

[39] Wang, T., & Hsu, T. T. C. (2001). Nonlinear finite element analysis of concrete structures using new constitutive models. Computers & Structures, 79(32), 2781–2791. doi:10.1016/s0045-7949(01)00157-2.